Soil Dynamics and Earthquake Engineering 136 (2020) 106213

Contents lists available at ScienceDirect

Soil Dynamics and Earthquake Engineering

journal homepage: http://www.elsevier.com/locate/soildyn

# Earthquake response of monopiles and caissons for Offshore Wind Turbines founded in liquefiable soil

Pourya Kazemi Esfeh [a], Amir M. Kaynia [b,c,*]

[a] Department of Civil, Chemical, Environmental, and Materials Engineering, University of Bologna (UNIBO), Italy
[b] Norwegian Geotechnical Institute (NGI), Norway
[c] Norwegian University of Science and Technology (NTNU), Trondheim, Norway

ARTICLE INFO

*Keywords:*
Liquefaction
Monopile
Caisson foundation
Seismic analysis
SANISAND constitutive Model
Offshore wind

ABSTRACT

Monopile has been the most widespread foundation type for Offshore Wind Turbines (OWTs) in shallow waters. Caisson (skirted) foundations have also been evaluated in some projects as an economical alternative. While the main concern in design of offshore foundations has been the environmental loads, the recent growth in construction of OWTs in seismic regions with the possibility of soil liquefaction has necessitated evaluation of the impact of earthquake and liquefaction from strong shakings on these structures. Several studies have reported the consequences of soil liquefaction for buildings and onshore structures; However, the effects of liquefaction on offshore foundations have not been sufficiently studied. This paper investigates the use of advanced liquefaction modeling in assessment of the response of monopiles and caissons for offshore wind turbines. The software FLAC3D and the SANISAND constitutive model are used to conduct the nonlinear dynamic analyses for OWTs. Excess pore water pressure during earthquake shaking and earthquake-induced displacements are computed at various points in the soil medium around the considered monopile and caisson foundations. The analyses reveal that SANISAND model is capable of simulating the pore pressure generation in the free-field as observed in a recent centrifuge test. The numerical results also indicate that both monopile and caissons in liquefiable soil deposits experience considerable rotations under the combined action of wind loads and earthquake shaking when liquefaction occurs.

## 1. Introduction

The interest in replacing fossil energy with renewable energy is constantly increasing. The offshore wind energy has become highly attractive over the past few years thanks to the higher and more stable wind speeds available offshore compared to onshore resulting in higher electricity generation. To highlight this fact, it is worth noting that the global offshore wind capacity grew to over 20 GW in 2018 [1] and the investment in offshore wind energy has continued to be massive. The interest in this source of energy has provided a significant incentive to evaluate use of various types of foundations for Offshore Wind Turbines (OWTs) in different water depths. Monopiles have been by far the most common foundations for OWTs in shallow waters (water depths less than about 50 m) (Fig. 1a). However, the use of monopiles in deeper waters could be conditional upon the weight of the pile and installation capabilities. For larger OWTs and deeper water, more cost-effective foundation types such as large diameter caissons (Fig. 1b), and moored floating structures have been investigated in recent years.

Since the majority of OWTs have been installed in areas with low seismicity (e.g. Northern Europe), the seismic analysis and liquefaction assessment have not been the primary concerns in design of these structures. However, the recent developments of OWT farms in seismically active areas with the possibility of soil liquefaction (e.g. East Asia, Southern Europe and USA) have necessitated a more critical evaluation of the effect of seismic loads and liquefaction due to strong shakings on these structures [2]. Several recent studies on the dynamic response of OWTs to the combined action of wind and earthquake shaking have reported the importance of seismic loading in design of these structures (e.g. Ref. [3–5]). Liquefaction could have a significant impact on OWT foundations in liquefiable sand deposits.

The permanent rotation (tilt) of OWT foundations resulting from the wind and wave loads acting on the turbine structure has been the paramount factor in the design of these structures. In earthquake-prone areas, earthquake shakings and soil liquefaction could lead to a

* Corresponding author. Norwegian University of Science and Technology (NTNU), Trondheim, Norway.
*E-mail addresses:* pooria.kazemi@studio.unibo.it (P.K. Esfeh), amir.m.kaynia@ngi.no (A.M. Kaynia).

https://doi.org/10.1016/j.soildyn.2020.106213
Received 16 January 2020; Received in revised form 29 March 2020; Accepted 4 May 2020
Available online 16 June 2020

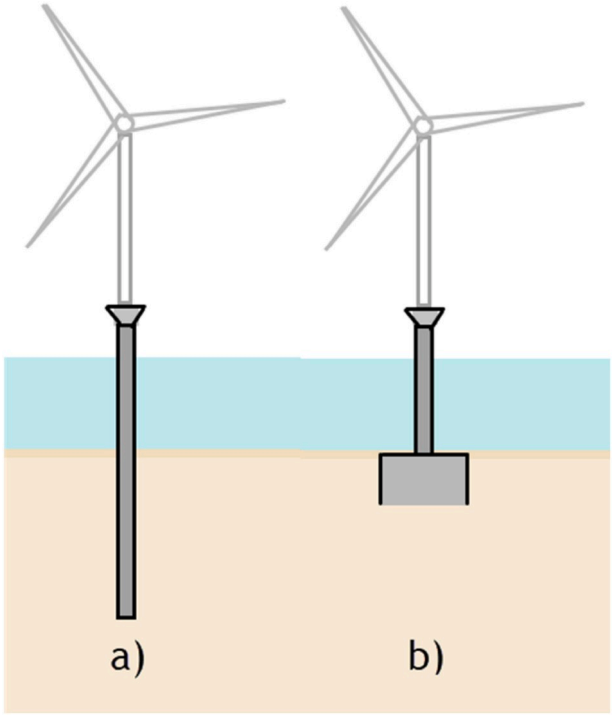


**Fig. 1.** Foundations for offshore wind turbines considered in this study: a) monopile b) caisson.

**Table 1**
Summary of soil sample properties used in triaxial tests [49].

| Property | Relative density $D_r$ (%) | | |
|---|---|---|---|
| | 40 | 60 | 90 |
| Void ratio, e | 0.69–0.7 | 0.64–0.65 | 0.55–0.56 |
| Hydraulic conductivity, k (m/s) | $1.41 \times 10^{-4}$ | $1.36 \times 10^{-4}$ | $1.19 \times 10^{-4}$ |
| Peak friction angle, $\varphi_p$ (degrees) | 32–32.5 | 34.8–36.5 | 41.5–42.1 |
| Phase transformation angle $\varphi_{PT}$ (degrees) | 25.1–31.2 | 24.5–30 | 22.2–28.5 |

**Table 2**
Summary of initial soil conditions in the centrifuge experiment [50].

| Thickness/$D_r$/Layer | e | $\gamma_{sat}$ (kN/m$^3$) | k (m/s) |
|---|---|---|---|
| 2 m/90%/Monterey | 0.57 | 19.8 | $5.30 \times 10^{-4}$ |
| 6 m/40%/Ottawa sand F65 | 0.7 | 19.1 | $1.41 \times 10^{-4}$ |
| 10 m/90%/Ottawa sand F65 | 0.56 | 19.9 | $1.19 \times 10^{-4}$ |

combination of permanent translational displacement and tilt of the foundations and threatening their stability and serviceability [2]. Moreover, pore pressure buildup produced in sand during the earthquake shaking may give rise to variation in soil stiffness and accordingly modifying the dynamics of the structure. The effect of liquefaction is believed to be more dramatic on bucket/caisson foundations since they have a smaller contact with the soil which might lead to significant permanent displacements/rotations in these foundations.

In the past few decades, laboratory tests (e.g. Ref. [6,7]), CPT-based and SPT-based liquefaction assessment procedures (e.g. Ref. [8,9]) and numerical modeling (e.g. Ref. [10–12]) have been carried out to evaluate liquefaction potential. However, despite extensive research on the topic, the number of studies on the effect of liquefaction on structures, specially OWT structures/foundations, is very limited.

Several studies have been conducted in recent years to improve the understanding of soil-monopile interaction under cyclic loading due to wind and wave loads. These studies have generally addressed soil-monopile lateral stiffness (e.g. Ref. [13–23]) and displacement/rotation accumulation after many loading cycles (e.g. Refs. [24–27]). Several of these studies have tried to improve the p-y methods with respect to the diameter effect and stiffness at small strains [23]. The p-y methods have been extended to dynamic analyses by determining proper hysteretic cyclic behavior for the springs (e.g. Ref. [28]) and considering additional elements to account for free-field response under seismic loading [29].

Finite Element/Finite Difference (FE/FD) methods have been employed for prediction of the pore pressure buildup in the liquefiable soil around OWT foundations and anchors by considering the effects of hydromechanical coupling in the saturated sand (e.g. Ref. [30–36]). In most of these studies, pore pressure generation has been assessed only under wind or wave loads [30,31,33,34] while only a few studies have focused on either the liquefaction and its consequences for OWT structures due to strong ground shaking or the performance of these structures under a combination of seismic and environmental loads (e.g. Refs. [32,35,36]). Corciulo et al. [31] and Kementzetzidis et al. [33] investigated the OWT-monopile-soil interaction and the effect of soil nonlinearity on the dynamic response of OWT structures founded on large monopiles. In these studies, the pore pressure buildup, stress paths and shear stress-strain responses were assessed in medium-dense/dense sand for different wind/wave loading conditions. Yang et al. [32] investigated the dynamic response of Lely OWT supported by a monopile with a diameter of 3.7 m under combined actions of wind loading and earthquake shaking. However, the monopiles currently used for OWTs have diameters ranging from 5 to 8 m supporting large OWTs with the power typically in the range 5–8 MW. Since the pile's diameter considerably affects the way in which the monopile interacts with the surrounding soil [23], investigation of the performance of larger OWT monopiles during liquefaction under various loading conditions is essential. Moreover, a sensitivity analysis highlighting the influence of the pile's length on the dynamic response of monopiles is of high interest. Fewer studies have been reported on the response of caissons subjected to earthquake loading and liquefaction. Research on caisson foundations have primarily focused on external cyclic loading, and considerable uncertainties hang over the performance of caissons under earthquake loading, especially during liquefaction. Kazemi Esfeh and Kaynia [35] focused on establishing a reliable computational model for liquefaction response of anchor piles. They investigated several modeling features including mesh size, lateral boundary conditions, solution using large displacements, and presented a verification of the calibrated material parametersin different soil tests.

A robust numerical modeling of liquefaction and its impact on structures requires advanced constitutive models. In recent years, several nonlinear elasto-plastic models have been developed for numerical simulation of site response, excess pore pressure and accumulation of shear/volumetric strain in soils susceptible to liquefaction (e.g. Ref. [37–41]). In this study, the Simple Anisotropic model for sand (SANISAND) developed by Dafalias and Manzari [38] and implemented in the finite difference software FLAC3D is used for performing dynamic analyses. The success of this constitutive model to simulate the response of saturated sand under cyclic loading has been demonstrated by element-level tests and centrifuge experiments in recent years (e.g. Ref. [42–46]).

Ziotopoulou [44] performed numerical predictions of the LEAP centrifuge tests [47] using the finite difference software FLAC and PM4Sand constitutive model [40]. The PM4Sand model parameters were calibrated against the centrifuge tests. The results of numerical simulations have indicated that PM4Sand is capable of simulating the dynamic response of sloping ground. Ramirez et al. [46] evaluated the predictive capabilities of SANISAND and PDMY02 [48] constitutive models used in the two numerical platforms OpenSess and FLAC. In their study, they validated the model parameters by using the results of element-level tests and a centrifuge experiment simulating the field response in a multi-layered liquefiable soil deposit.

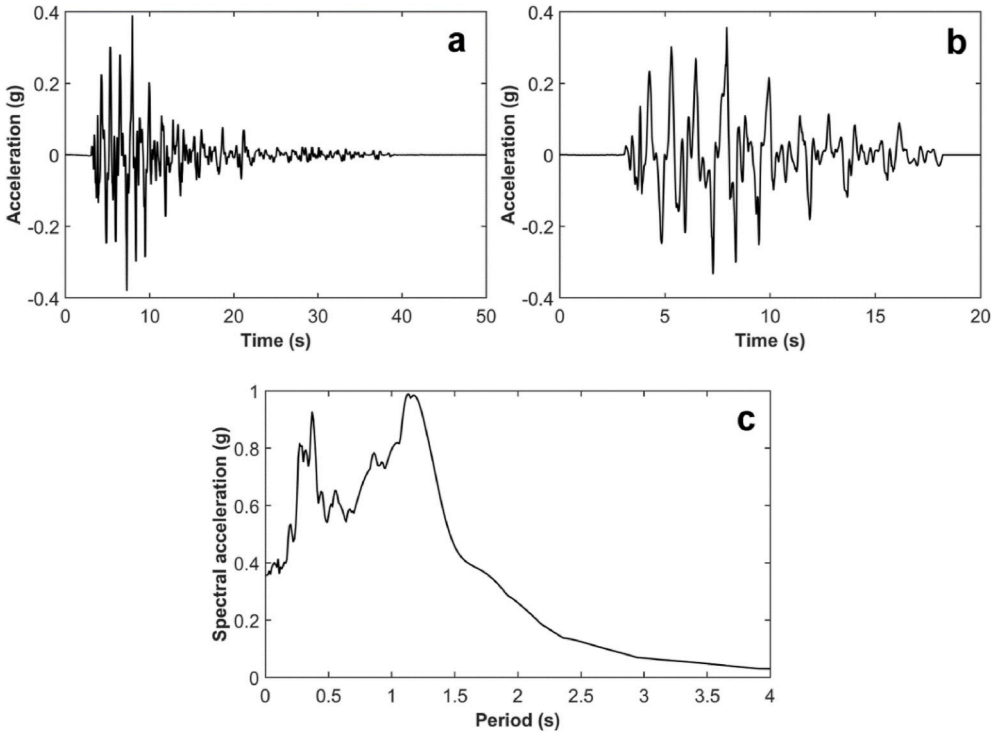


**Fig. 2.** Acceleration time history of Kobe-L earthquake applied at a) base of container [50] b) base of caisson/monopile numerical models and c) corresponding acceleration response spectrum (5% damping).

**Table 3**
SANISAND constitutive model parameters calibrated for Ottawa sand F65 [46].

| Parameter | Value | |
|---|---|---|
| | Ottawa | Monterey |
| Nondimensional elastic modulus factor, $G_0$ | 125 | 130 |
| Poisson's ratio, $\upsilon$ | 0.05 | 0.05 |
| Critical state stress ratio, M | 1.26 | 1.27 |
| Ratio of critical-state stress ratio in extension and compression, c | 0.735 | 0.712 |
| State line constant, $\lambda_c$ | 0.0287 | 0.02 |
| Void ratio at p = 0, $e_0$ | 0.78 | 0.858 |
| State line constant, $\xi$ | 0.7 | 0.69 |
| Yield surface constant, m | 0.02 | 0.02 |
| $h_0$ | 5 | 8.5 |
| $c_h$ | 0.968 | 0.968 |
| $n^b$ | 0.6 | 1.05 |
| $A_0$ | 0.5 | 0.6 |
| $n^d$ | 0.5 | 2.5 |
| $z_{max}$ | 11 | 4 |
| $c_z$ | 500 | 50 |
| $\bar{e}^p_{eq}$ | 0.01 | 0.01 |
| $N$ | 1 | 1 |

In the present study, the finite difference software FLAC3D and constitutive model SANISAND with the same parameters proposed by Ramirez et al. [46] are used to conduct dynamic soil-structure interaction analyses of OWTs. The study builds on the computational model in Ref. [35] and investigates the influence of liquefaction on the seismic response of large OWTs on both monopiles and caissons with different dimensions subjected to a combination of static/cyclic wind load and earthquake shaking. To gain insight into the performance of monopiles and caissons during liquefaction, the pore pressure buildup, the shear stress-strain responses and the earthquake-induced displacements at several points in the soil medium are computed and presented.

## 2. Validation of numerical model

Ramirez et al. [46] calibrated the SANISAND constitutive model parameters in FLAC with a series of strain-controlled undrained/drained monotonic/cyclic triaxial tests together with a centrifuge experiment simulating the site response in a liquefiable sand deposit. In the present study, FLAC3D was employed to confirm these model parameters by comparing the experimental and numerical results of a series of monotonic/cyclic triaxial tests. Consequently, the 3D site response was evaluated using the results of the centrifuge experiment. The main objective was to use the calibrated model parameters in the numerical simulation of the earthquake responses of monopiles and caissons during liquefaction.

### 2.1. Triaxial tests

A series of strain-controlled undrained/drained cyclic/monotonic triaxial tests on Ottawa sand F65 (silica sand classified as SP based on USCS) was conducted by Ramirez et al. [49]. The results of these tests were used by Ramirez et al. [46] to calibrate the SANISAND constitutive model parameters. All sand specimens were prepared by air pluviation at three relative densities $D_r$ = 40%, 60% and 90%. For the drained monotonic triaxial compression tests, all specimens were isotropically consolidated to three levels of confining pressures 100, 200 and 300 kPa. For the undrained monotonic triaxial compression tests with the same set of relative densities, the isotropic effective stresses were 50, 100 and 200 kPa. All samples for cyclic undrained triaxial tests were isotropically consolidated to a confining pressure of 100 kPa. Table 1 summarizes the soil properties used in the triaxial tests.

### 2.2. Centrifuge experiment

Results of the centrifuge test with the free-field condition (i.e. no structure) conducted at the University of Colorado Boulder's 5.5 m centrifuge facility [50] were used to validate the numerical model of the site response during earthquake shaking. The 18-m soil profile contains

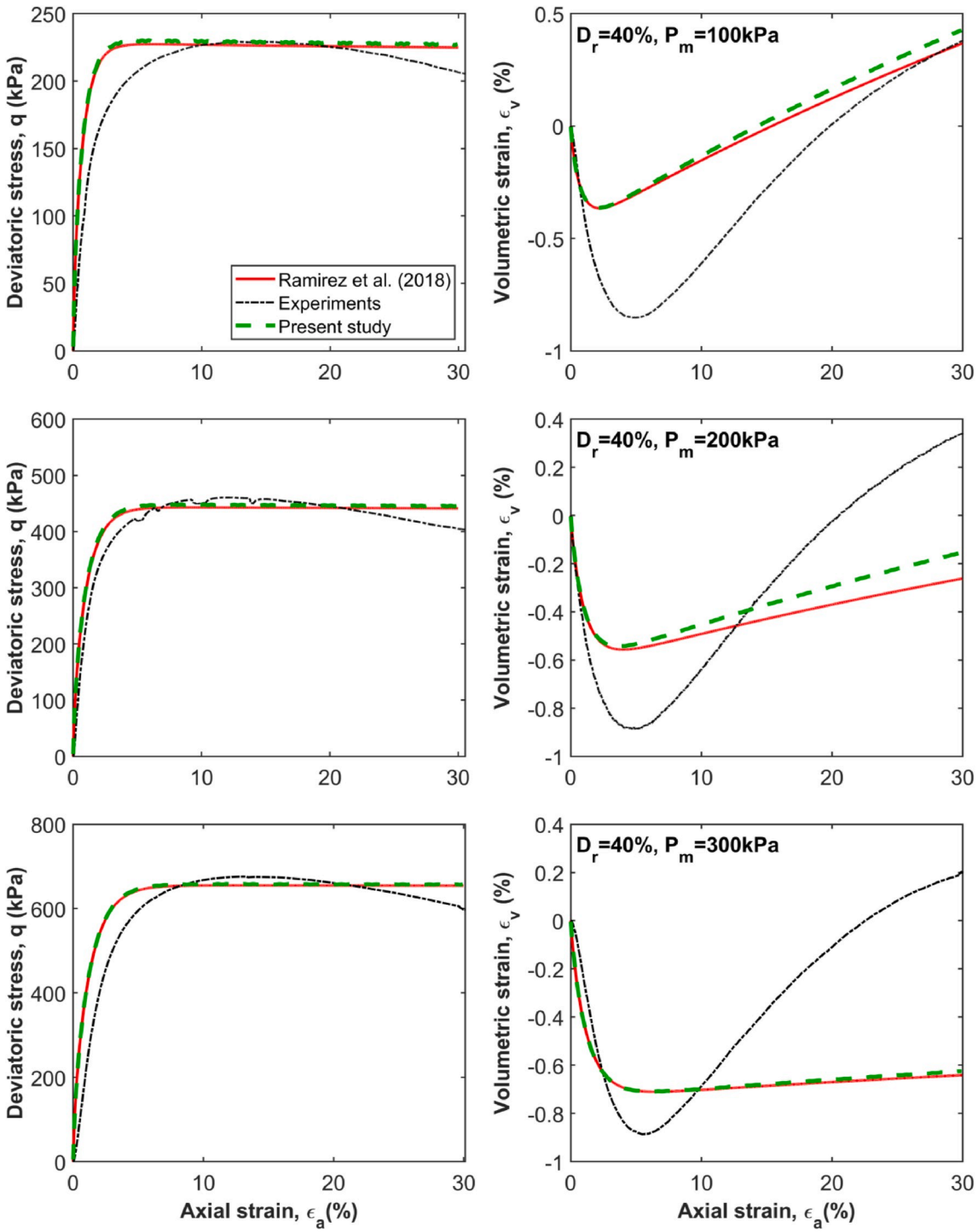


**Fig. 3.** Comparison between numerical and experimental results for simulations of monotonic drained triaxial tests on loose Ottawa sand with $D_r$ = 40%.

10 m of dense Ottawa sand with $D_r = 90\%$ at the bottom, 6 m of loose Ottawa sand with $D_r = 40\%$ as the liquefiable layer in the middle and 2 m of Monterey sand with $D_r = 90\%$ on the top. The soil properties used in the centrifuge test are listed in Table 2. Accelerograms, pore-pressure transducers and vertical LVDTs were installed at different depths in the soil profile (z = −18, −13, −8, −5 and −2 m) to measure the accelerations, pore pressures and vertical displacements during the shaking. The model was spun to a nominal centrifugal acceleration of 70g.

A series of horizontal earthquake motions were applied to the base of the container among which the Kobe-L earthquake was considered for the numerical simulation in the present study. This earthquake record is a scaled version of the north-south fault normal horizontal component of the 1995 Kobe, Japan, earthquake recorded at the Takatori station with PGA = 0.41g. The acceleration time history and its corresponding acceleration spectrum (for 5% damping) are illustrated in Fig. 2a.

### 2.3. Numerical analyses

The fully dynamic analyses in this paper were performed using the finite difference software FLAC3D. The calculation was based on the explicit finite difference scheme to solve the equations of motions using

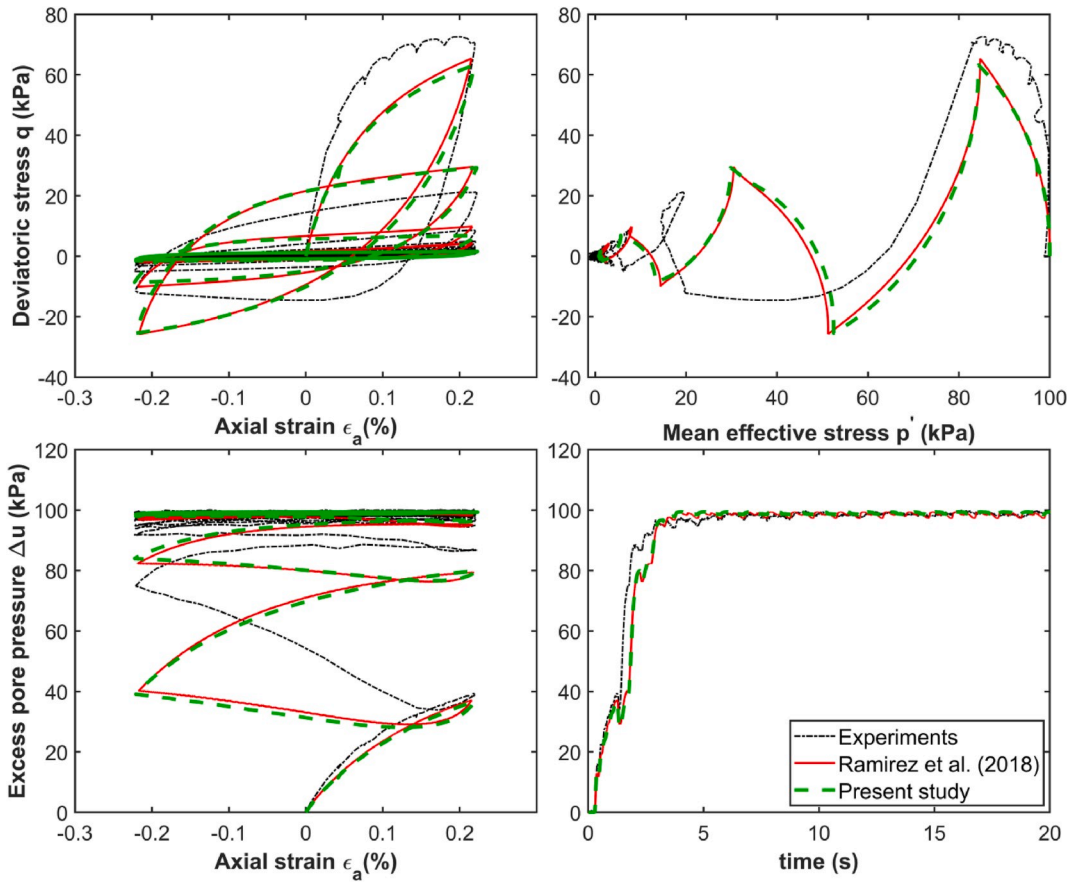


**Fig. 4.** Comparison between numerical and experimental results for simulations of cyclic undrained triaxial tests on Ottawa sand with $D_r$ = 40%.

the lumped gridpoint masses of the surrounding zones. The dynamic analyses in FLAC3D can be coupled with groundwater flow analyses to predict time-dependent pore pressure changes during the liquefaction. FLAC3D follows the coupled formulations of poro-mechanics proposed by Biot [51], extended to finite elements by Zienkiewicz and Shiomi [52] and presented for application in FLAC by Detournay and Cheng [53]. The bulk modulus and density of water were respectively taken as 2 GPa and 1000 kg/m$^3$ in the simulations.

The SANISAND constitutive model was used in FLAC3D to simulate the soil's behavior under cyclic loading. SANISAND refers to a family of simple anisotropic constitutive models for sand extended from the two-surface plasticity model which was first developed by Manzari and Dafalias [54]. The model was later extended by other researchers to consider additional features of sand's behavior in various loading conditions. The SANISAND constitutive model that was extended by Dafalias and Manzari [38] to account for the effect of fabric change was employed in the present study. Despite the principal merits of SANISAND (e.g. capturing the effects of varying confining pressures and void ratios, modeling fabric changes due to load reversal, and simulating contractive and dilative behavior of sand), this constitutive model has certain intrinsic shortcomings. For instance, the model is known to overpredict the pore pressure buildup rate in medium-dense and dense sand as well as strain accumulation under high-cyclic loading. Therefore, although the trends of the results presented in this study are believed to be correct, the numerical values should primarily be used in a comparative sense. Table 3 lists the SANISAND model parameters calibrated by Ramirez et al. [46] for both Ottawa and Monterey sand.

### 2.4. Calibration of model parameters

Ramirez et al. [46] calibrated the SANISAND model parameters against monotonic/cyclic (drained/undrained) triaxial tests [49] and the centrifuge experiment [50]. In the present study, these model parameters were confirmed using FLAC3D. A sample of the results of some of the verifications carried out in this study is presented below.

A comparison of numerical and experimental results of monotonic drained triaxial tests for loose Ottawa sand performed in the present study is illustrated in Fig. 3. It can be observed that SANISAND correctly captures the initial stiffness, peak deviatoric strength and softening behavior of loose sand under the considered range of confining pressures. In general, the stress-strain responses predicted in the present study using FLAC3D are close to those reported in Ref. [46] .

Fig. 4 presents a comparison between numerically computed and experimentally measured results of cyclic undrained triaxial tests for loose sand. There is a reasonably good agreement between the two results in terms of excess pore water pressure and stress-strain response for loose sand. A closer look at Fig. 4 also confirms that the results of the present study using FLAC3D are very similar to those obtained by Ramirez et al. [46] . For more information about the model validations see Ref. [35].

### 2.5. Simulations of centrifuge test

To simulate the elasto-plastic site response of the soil in the centrifuge experiment, a soil column with tied boundary conditions was used in FLAC3D. While the tied boundary condition represents best the laminated box in the centrifuge and it produced the most accurate results, the effect of quiet (viscous) boundaries was also examined. The latter boundary condition did not consistently reproduce the site response measured in the centrifuge test. The SANISAND model parameters summarized in Table 3 were assigned to the soil layers. A Rayleigh damping with damping ratio $\xi$ = 3% at the first and third

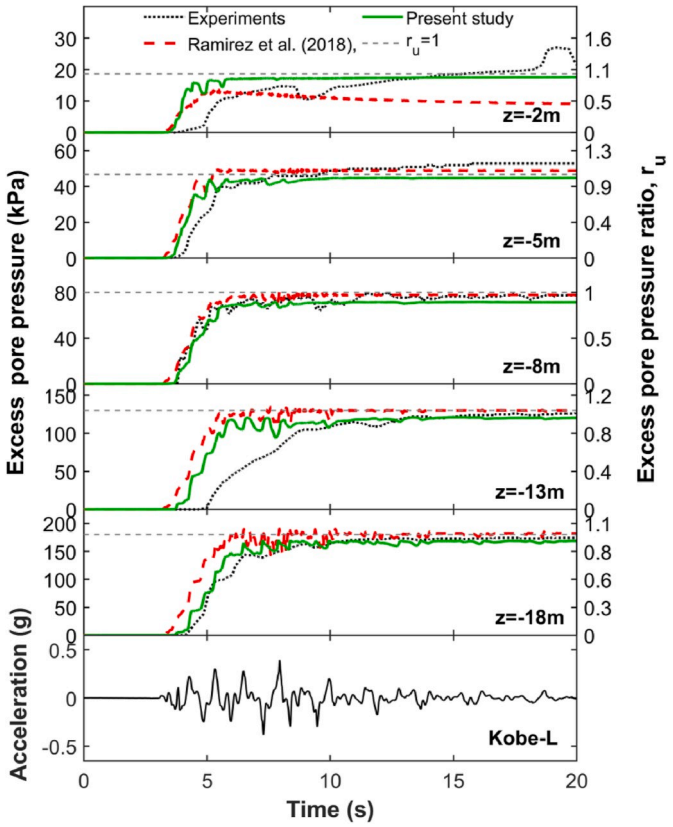


**Fig. 5.** Comparison of numerically calculated and experimentally measured time histories of excess pore pressures for simulations of site response in centrifuge experiment.

natural frequencies of the soil deposit, $f_{n,1} = 2.5$ Hz and $f_{n,3} = 12.3$ Hz, was used for the dynamic analysis of the soil in the centrifuge test. The acceleration time history in Fig. 2a was applied at the base of the model.

Fig. 5 compares the numerical and experimental excess pore pressures at several points in the soil profile together with the results in Ref. [46]. The excess pore pressure is also presented in terms of excess pore pressure ratio $r_u = \Delta u/\sigma'_{v0}$(where $\sigma'_{v0}$ is the initial effective vertical stress). The limit $r_u = 0.95$ was regarded as liquefaction criterion. A closer look at Fig. 5 reveals that pore pressures recorded in the centrifuge experiment of Kirkwood and Dashti [50] lag at depth 13 m. This might be due to an error in the data acquisition at this particular sensor.

## 3. Numerical modeling of OWTs on caisson and monopile

### 3.1. Model parameters and loading

The constitutive model and finite difference scheme described in the previous sections were employed to assess the dynamic response of caisson and monopile foundations for OWTs in a liquefiable sand deposit due to earthquake shaking. The representative wind turbine considered for this study was the *NREL* 5-MW *offshore baseline wind turbine* (Fig. 6). This is a reference offshore wind turbine defined by National Renewable Energy Laboratory (NREL) for researchers to use as a common reference model in their studies [55]. It is a three-bladed upwind horizontal axis wind turbine (HAWT) with a monopile support structure. The data for this wind turbine are summarized in Table 4.

The quadrilateral element in FLAC3D was used to model the soil, caisson, monopile and the tower of the wind turbine. Due to symmetry, only half of the soil medium, foundation and OWT model was considered with appropriate boundary conditions specified on the symmetry plane. The mesh size was based on the sensitivity studies in [35] and

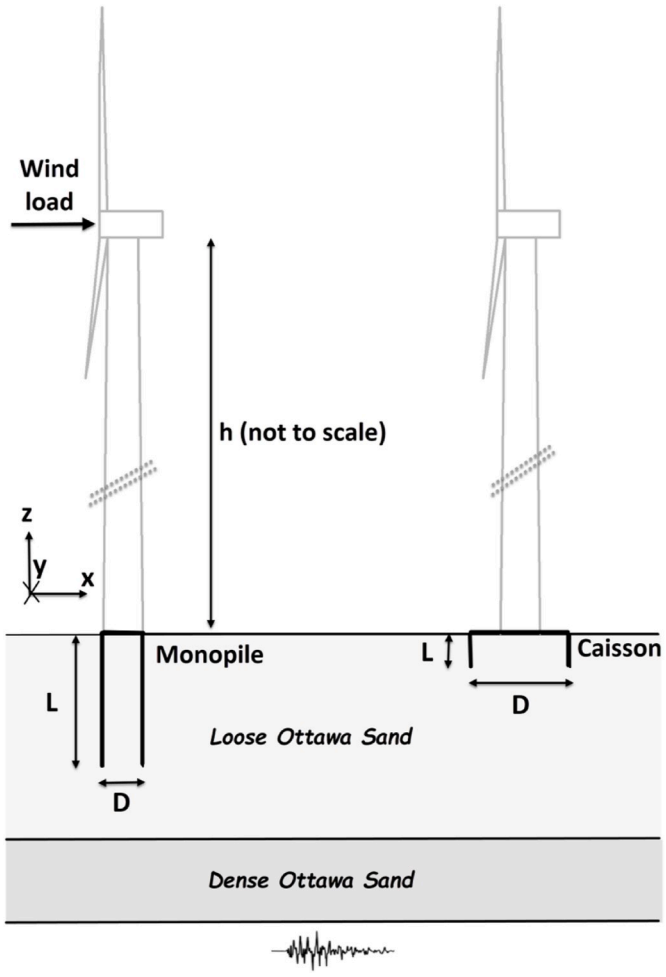


**Fig. 6.** Schematics of *NREL* 5-MW *offshore baseline wind turbine* founded on monopile (left) and caisson (right). See Table 4 for parameters.

**Table 4**
Properties of NREL 5-MW baseline wind turbine.

| Property | Value |
|---|---|
| Rating | 5 MW |
| Rotor orientation, configuration | Upwind, 3 blades |
| Rotor diameter, hub diameter | 126 m,3 m |
| Hub height | 90 m |
| Cut-in, rated, cut-out wind speed | 3 m/s, 11.4 m/s, 25 m/s |
| Cut-in, rated rotor speed | 6.9 rpm,12.1 rpm |
| Rated tip speed | 80 m/s |
| Rotor mass | 110 000 kg |
| Nacelle mass | 240 000 kg |
| Tower mass | 347 466 kg |
| Tower height | 87.6 m |
| Tower top diameter, wall thickness | 3.87 m, 0.019 m |
| Tower base diameter, wall thickness | 6 m, 0.027 m |
| Substructure base diameter, wall thickness | 6 m, 0.06 m |
| Support structure steel density | 8500 kg/m$^3$ |
| Steel Young's modulus | 210 GPa |

aimed at allowing 10 elements in a wavelength corresponding to a frequency of 10 Hz (period of 0.1 s in Fig. 2c) and elastic shear modulus. Once the soil liquefies, the effective shear modulus reduces but the dominant frequency reduces as well. This is a complicated process; however, considering that the dominant frequency range of input motion is in the range 0.7–2 Hz (see Fig. 2c), the selection of maximum frequency 10 Hz was considered to be satisfactory also during the liquefaction as comparisons with centrifuge results confirm. Tied

**Table 5**
Properties of caisson and monopile foundations.

| Foundation type | Diameter, D (m) | Length, L (m) | Equivalent unit mass, $\rho_{eq}$ (kg/m$^3$) | Equivalent elastic modulus, $E_{eq}$ (GPa) |
|---|---|---|---|---|
| Caisson | 10 | 5 | 2480 | 19.4 |
| | 15 | 5 | 2480 | 18.5 |
| Monopile | 6 | 20 | 2500 | 21.3 |
| | 6 | 25 | 2500 | 21.3 |
| | 6 | 35 | 2500 | 21.3 |

boundary conditions were found to provide the most stable results [35].

With the purpose of evaluating the effect of liquefaction on the performance of common foundation concepts for OWTs, the caissons and monopiles (Fig. 6) with typical dimensions listed in Table 5 were considered in this study (see discussion in the next paragraph for the material parameters). Similar caisson and monopile sizes were used in [56]. Sensitivity analyses were carried out to determine the optimum size of the models for the best performance (Figs. 7 and 8). The same soil profile as in the centrifuge test was used when assessing the OWT on caissons. On the other hand, the soil profile considered for OWT on monopile included 26 m of loose Ottawa sand on the top and 8 m of dense Ottawa sand at the bottom. For the pile model with length L = 35 m (see analysis cases described in the next section), the thickness of the dense Ottawa sand layer was extended to 13 m. The Rayleigh damping was defined based on 3% damping at the first and third natural frequencies of the soil deposit which were computed equal to $f_{n,1} = 1.25$ Hz and $f_{n,3} = 6.25$ Hz, respectively.

The linear elastic model with Young's modulus $E_{steel} = 210$ GPa and density $\rho_{steel} = 7800$ kg/m$^3$ was assigned to the steel parts (i.e. foundation and wind turbine structures). To avoid large aspect ratios of elements, the wall thickness of the pile was increased from 4 cm to 50 cm and correspondingly the elastic modulus and mass density of the pile were reduced. The equivalent elastic modulus $E_{eq}$ and mass density $\rho_{eq}$ were determined such that the bending rigidity and total mass of the equivalent pile (and skirt in the case of caisson) are equal to those of the real foundations (see [35] for details of the model adjustements). Different equivalent elastic moduli and unit masses resulted from this procedure depending on the diameter of the foundations, as listed in Table 5.

A fully bonded soil-pile interface was considered in all simulations such that nonlinearity at the interface occurs only due to loss of strength in sand during liquefaction. In [35] it was observed that the reduction of the shear strength at the soil-structure interface to 80% had only a minor

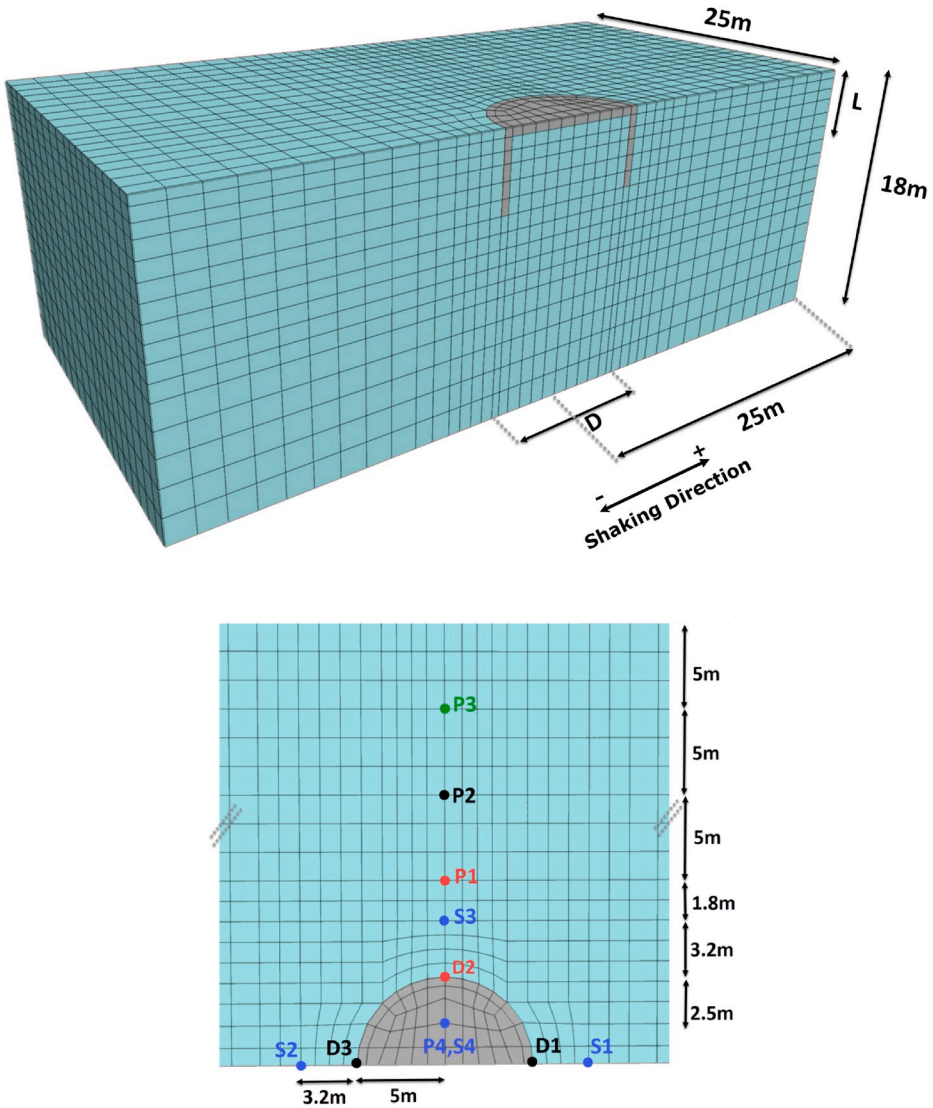


**Fig. 7.** a) Finite difference mesh of caisson model, b) monitoring points for computing excess pore pressures, shear stress-strain responses and displacements of caisson.

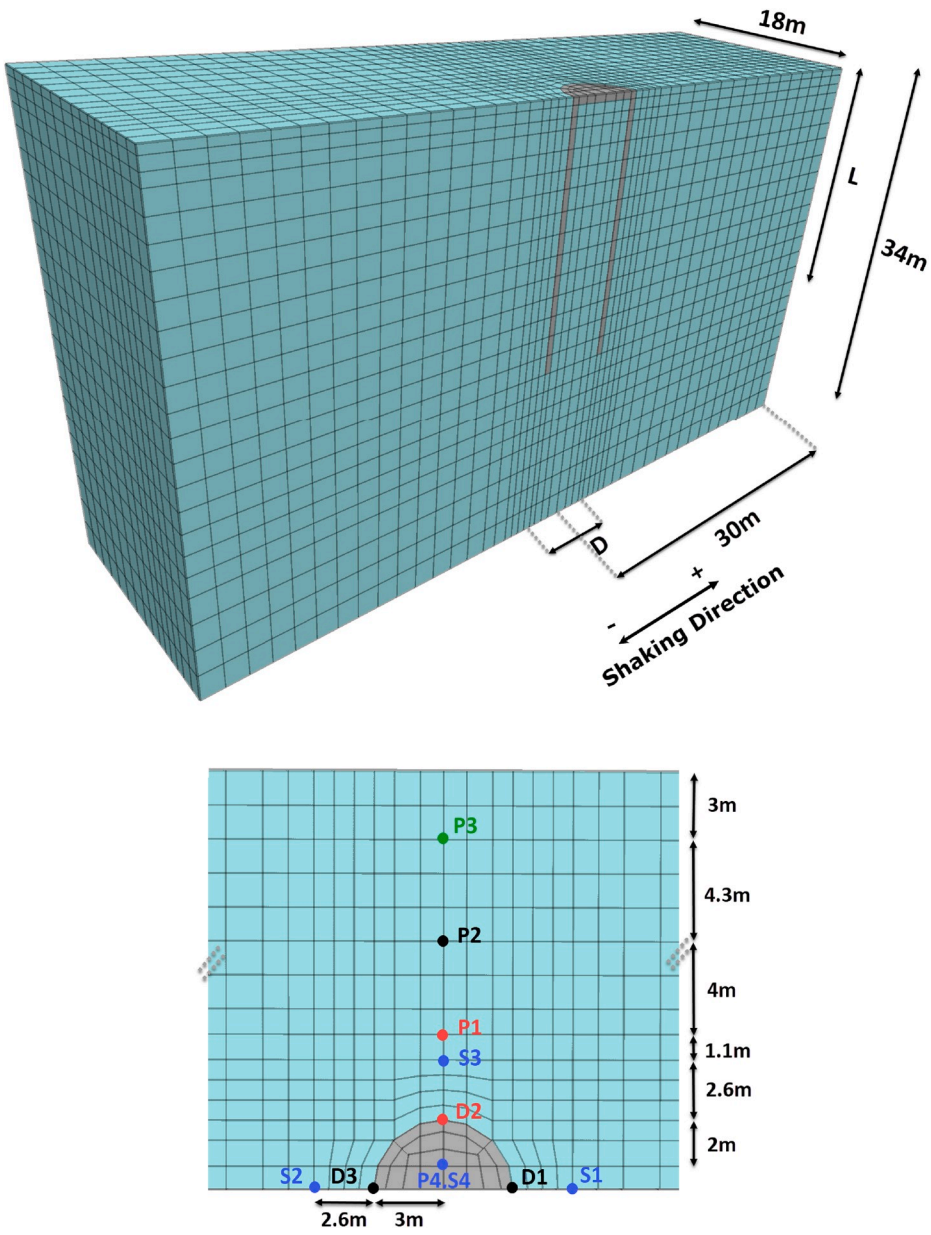


**Fig. 8.** a) Finite difference mesh of monopile model, b) monitoring points for computing excess pore pressures, shear stress-strain responses and displacements of pile.

effect on the results. Therefore, the soil-pile interface condition was not studied any further in this study.

The tapered cylindrical tower of the wind turbine with properties summarized in Table 4 was modelled as a uniform square column of solid zones in FLAC3D with dimensions of 2 m and element size of 1 m The elastic modulus $E_{eq}$ and unit mass $\rho_{eq}$ of the square column (equivalent tower) were established in a way to maintain the same lateral stiffness and total mass as those of the real tapered cylindrical tower. To this end, the elastic modulus $E_{eq}$ of the equivalent tower was defined in a way that its deflection due to a lateral force on top is equal to that of the real tower. The unit mass $\rho_{eq}$ of the equivalent tower was determined to match the real tapered tower. The mass of the hub (including nacelle and blades) was modelled as a lumped mass at the top of the tower by increasing the density of the last row of zones at the top of the tower.

The following loading scenarios were used for dynamic simulations.

Type A: combination of earthquake shaking and static wind loads

Type B: combination of earthquake shaking and simplified cyclic wind loads

Type C: only earthquake shaking (no wind load).

Loading types A and B were chosen to represent extreme loading scenarios that can occur in a highly seismic region, resulting in excessive lateral and rotational displacements due to simultaneous action of lateral loads. Loading type C was selected to highlight what portion of the computed permanent lateral displacement and tilt of the OWT foundation is due to the wind load.

Moreover, to assess the response of OWT foundations in liquefiable sand due to less severe earthquake shaking, which could represent moderate seismicity, the response of one of the cases considered in this study was also computed by reducing the shaking by 70%.

The Kobe-L earthquake record, which was applied at the base of the container in the centrifuge test, was used in dynamic simulations of the caisson and monopile models after baseline-correction and filtering (Fig. 2b). A static wind load of H = 1 MN (load Type A) and a simplified

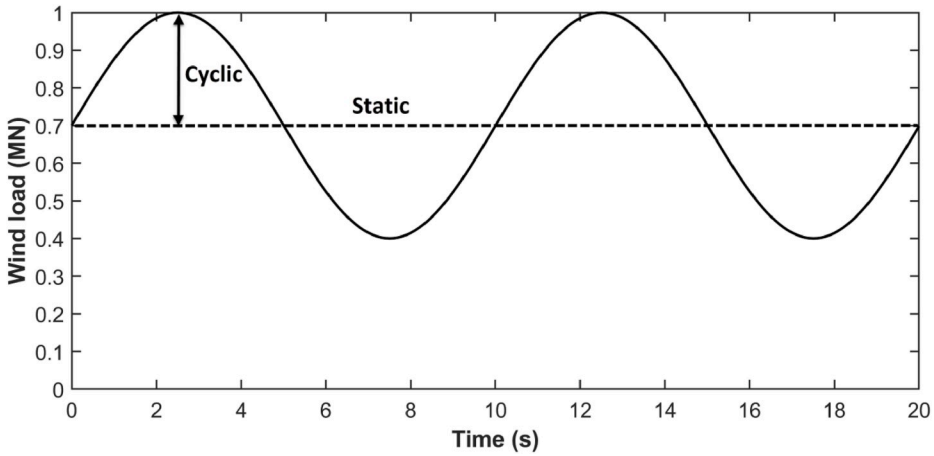


**Fig. 9.** Cyclic wind load applied to top of tower in numerical simulations.

**Table 6**
Average effective overburden stresses at different depths in soil model in Monopile Case 1 before earthquake shaking.

| Depth (m) | Average original effective overburden stress (kPa) | Average additional effective overburden stress (kPa) | Average initial effective overburden stress (kPa) |
|---|---|---|---|
| 4 | 38.52 | 0.48 | 39 |
| 8 | 74.7 | −3 | 71.7 |
| 16 | 122.9 | 7.26 | 130.2 |
| 24 | 154 | 48.9 | 202.9 |
| 30 | 252.6 | 5.28 | 257.9 |

cyclic wind load $0.7 + 0.3\sin(2\pi ft)$ MN (load Type B) with a frequency f = 0.1 Hz (Fig. 9) were applied to the top of the tower simultaneously with the earthquake motion at the base of the model. Wind load is generally complex due to its static and turbulent components and has a large spectrum of frequencies. The intention of selecting the frequency f = 0.1 Hz for the cyclic load was primarily to perform a sensitivity analysis on the effect of external load variation rather than attempting an exact representation of the wind load. The cyclic wind load was applied for 20 s while the earthquake shaking ends at 18 s.

In the computations, first, the flow mode was activated to establish the initial pore pressure distribution in the free-field. Afterward, flow mode was turned off during the application of wind load and earthquake shaking for the proper generation of pore water pressure. This means the response is considered undrained. In reality, the pore water pressure could change due to drainage; however, this is considered to be negligible in most sands during the short time of earthquake shaking. In all the simulations, monopile and caisson were considered impermeable; therefore, the null fluid constitutive model and zero porosity were assigned to their zones. In a sensitivity analysis performed in [35], the results of dynamic simulations in both small-strain and large-strain modes were compared. These results were found out to be very similar indicating that the small-strain assumption is satisfactory for the range of response computed in this study. Therefore, the dynamic simulations were conducted using small-strain solution to reduce the computational time.

### 3.2. Analysis cases and monitoring of response

To follow the soil response as the shaking continues and liquefaction develops, the excess pore water pressures at monitoring points P1–P4 (perpendicular to the shaking direction, as shown in Figs. 7b and 8b) were computed. In addition, in two of the analysis cases, the excess pore water pressures at two points behind and in front of the pile (located at a distance of 1.3 m from the pile) were computed. The average of the effective vertical stresses computed at monitoring points was used as the initial effective vertical stress ($\sigma'_{v0}$) before the earthquake shaking to calculate excess pore pressure ratios at each depth These stress values are listed in Table 6.

The soil inside the pile or caisson is under greater confining pressure and is therefore capable of generating larger pore pressures for sufficiently strong shaking; however, the normalized exces pore pressure could reduce because of the larger effective vertical stress. At the same time, a different mechanism, namely the kinematic confinement of the soil due the large stiffness of the foundation, which could inhibit/reduce the shear strains in the soil inside the foundation, is expected to reduce the excess pore pressures. Point P4 was thus chosen to investigate the possible reduction in pore pressure build-up within the inner soil due to the kinematic confinement by the monopile/caisson.

To assess shear strain accumulation around and inside the monopile/caisson during liquefaction, the shear stress-strain responses were computed at the points S1–S4. Similarly, horizontal and vertical displacements at points D1-D3 on top of the caisson/monopile were monitored to evaluate the transient and permanent displacements of the foundations during the earthquake. The foundation tilt was calculated using vertical displacements at points D1 and D3. Although during the shaking an OWT foundation can experience a considerable settlement, it is the rotation of the foundation that is the main cause of concern about its performance. Permanent rotation in the range 0.25–0.5 degrees is often acknowledged by design guidelines as the allowable range.

To gain insight into the performance of caissons and monopiles with different dimensions in a liquefiable soil, the following analysis cases were considered.

Caisson Case 1: diameter D = 10 m, loading type A
Caisson Case 2: diameter D = 10 m, loading type B
Caisson Case 3: diameter D = 15 m, loading type A
Monopile Case 1: length L = 20 m, loading type A
Monopile Case 2: length L = 25 m, loading type A
Monopile Case 3: length L = 25 m, loading type B
Monopile Case 4: length L = 35 m, loading type A
Monopile Case 5: same as Monopile Case 1 with Monterey sand on top
Monopile Case 6: length L = 25 m, loading type C (i.e. no wind loading).

In the last case, a section of the liquefiable sand with a depth of 2 m from the top and a radius of 9 m from the center of the model was replaced with dense Monterey sand before the monopile installation. The intention with this case was to investigate the impact of a non-liquefiable scour protection layer around the monopile. Moreover, the higher hydraulic conductivity of Monterey sand compared to that of Ottawa sand could facilitate the pore pressure dissipation after the earthquake, thereby reducing the consequences of pore pressure buildup

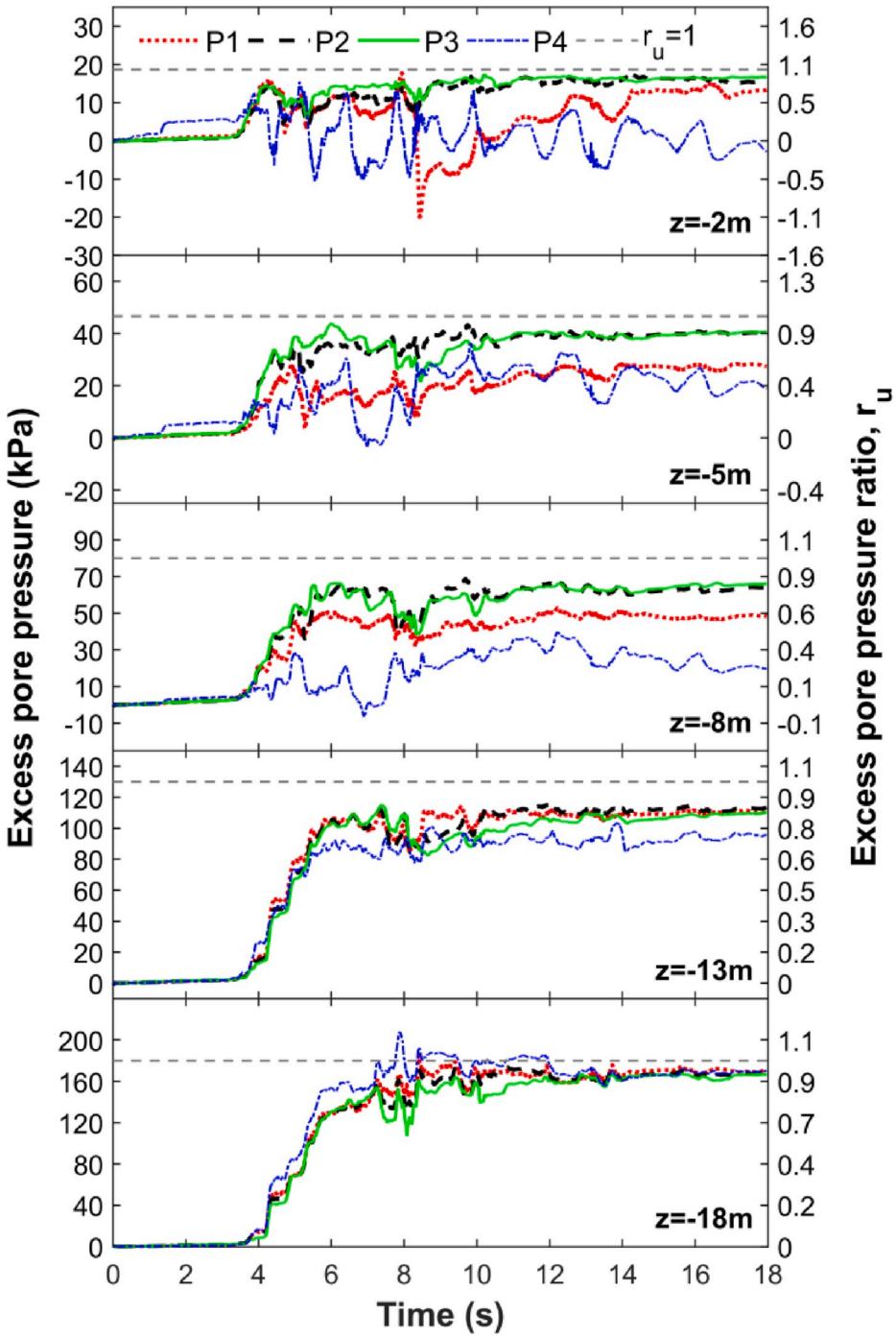


**Fig. 10.** Time histories of excess pore pressure at monitoring points in Caisson Case 1.

during earthquake.

The dynamic analyses were carried out using a PC with a 3.5 GHz processor. The simulations were speeded up by optimizing the model and mesh sizes as well as using small-strain solution. Increasing the thickness of the pile wall and caisson skirts, on the other hand, assisted in reducing the run times remarkably. With these measures, each simulation took from 20 to 30 h depending on the size of the model.

## 4. Results and discussions

The performance of monopile and caisson foundations during the liquefaction was evaluated in terms of pore water pressure buildup and shear stress-strain responses in the soil as well as the horizontal, vertical and rotational movements of the foundations.

### 4.1. OWT on caissons

Fig. 10 displays the time histories of the excess pore water pressures at different points and depths in the soil medium for Case 1. As the plots in the figure indicate, excess pore pressure ratios at all points and depths tend to one. Fig. 11 displays profiles of $r_u$ at monitoring points and four instances 4, 8, 12 and 16 s for the same case. It can be observed that the excess pore water pressure is almost all the time lower inside the caisson which is believed to be due to the kinematic confinement provided by the caisson.

Fig. 12 presents the computed acceleration time history together

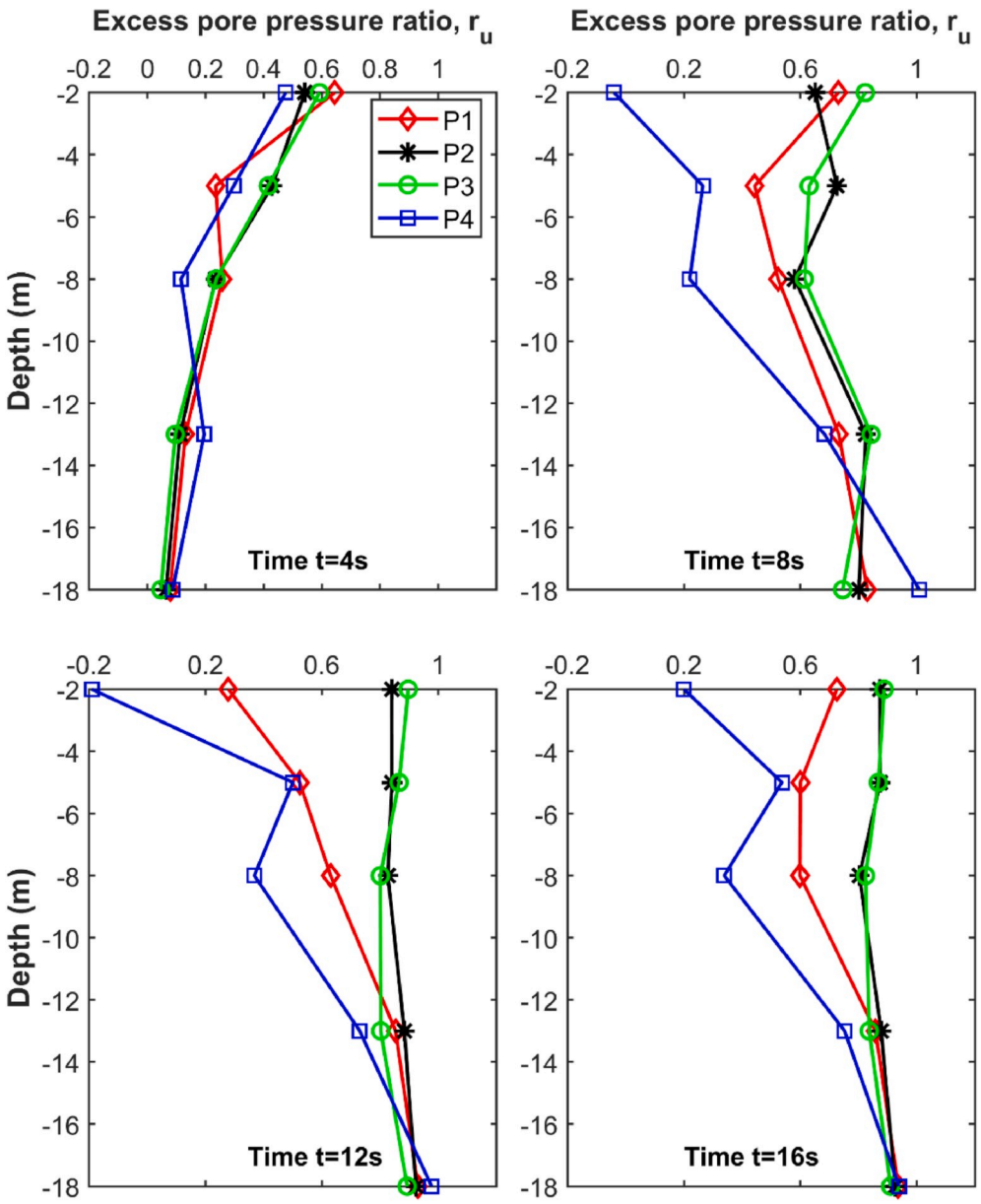


**Fig. 11.** Profiles of $r_u$ at different monitoring points and time instances in Caisson Case 1.

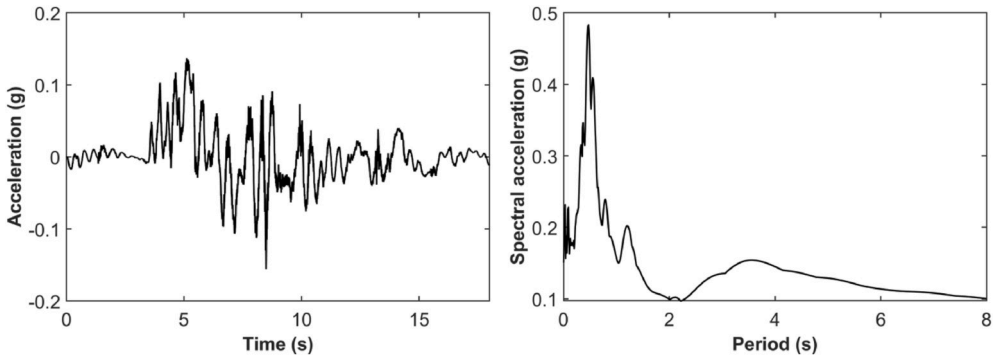


**Fig. 12.** Acceleration response at top of tower in Caisson Case 1.

with its response spectrum at top of the tower. A de-amplification of acceleration is observed which reflects the low spectral acceleration of the earthquake record at the natural period of the OWT-soil-caisson system [57] being around 3 s.

Figs. 13 and 14 display the shear stress-strain responses at monitoring points at depths z = −4 m and z = −2 m during the ground shaking. Different colors are used to differentiate between the responses in the time windows 0–6 s, 6–12 s and 12–18 s. The plots clearly show the shift in the response pattern from more conventional hysteretic and symmetrical responses (blue segments) to more yielding response due to

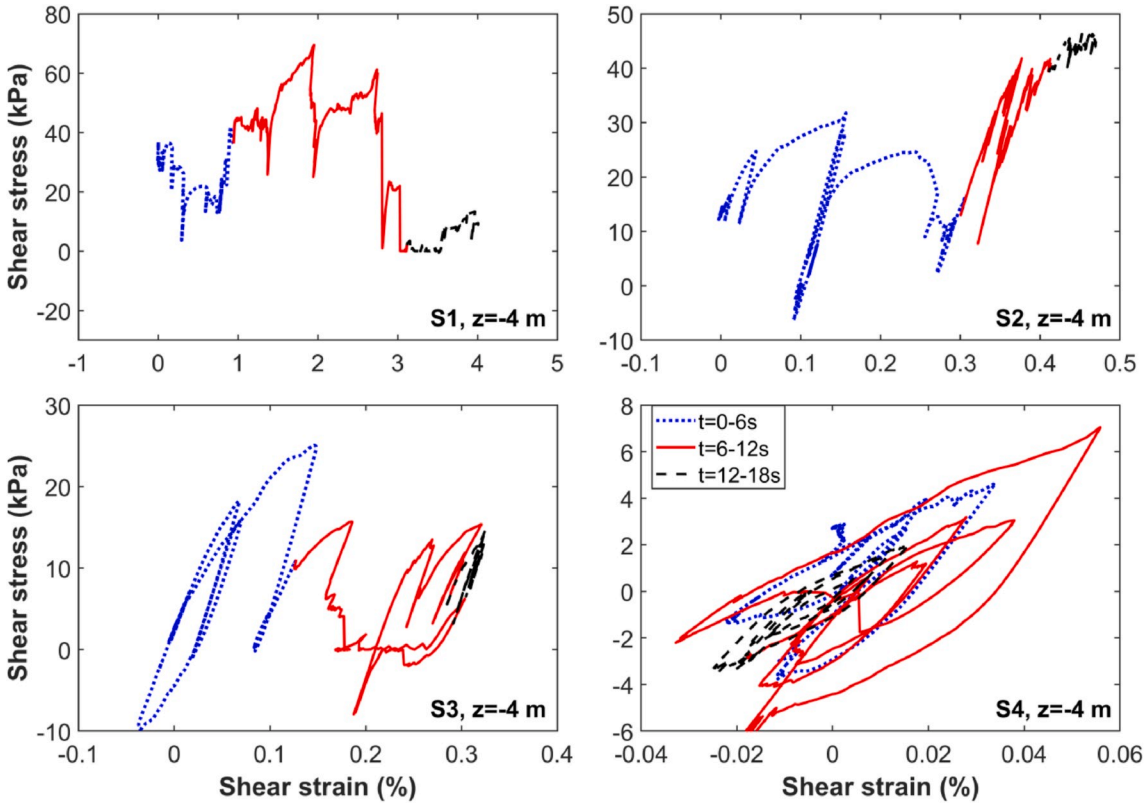


**Fig. 13.** Shear stress-strain responses at monitoring points and depth z = −4 m in Caisson Case 1 for different time periods.

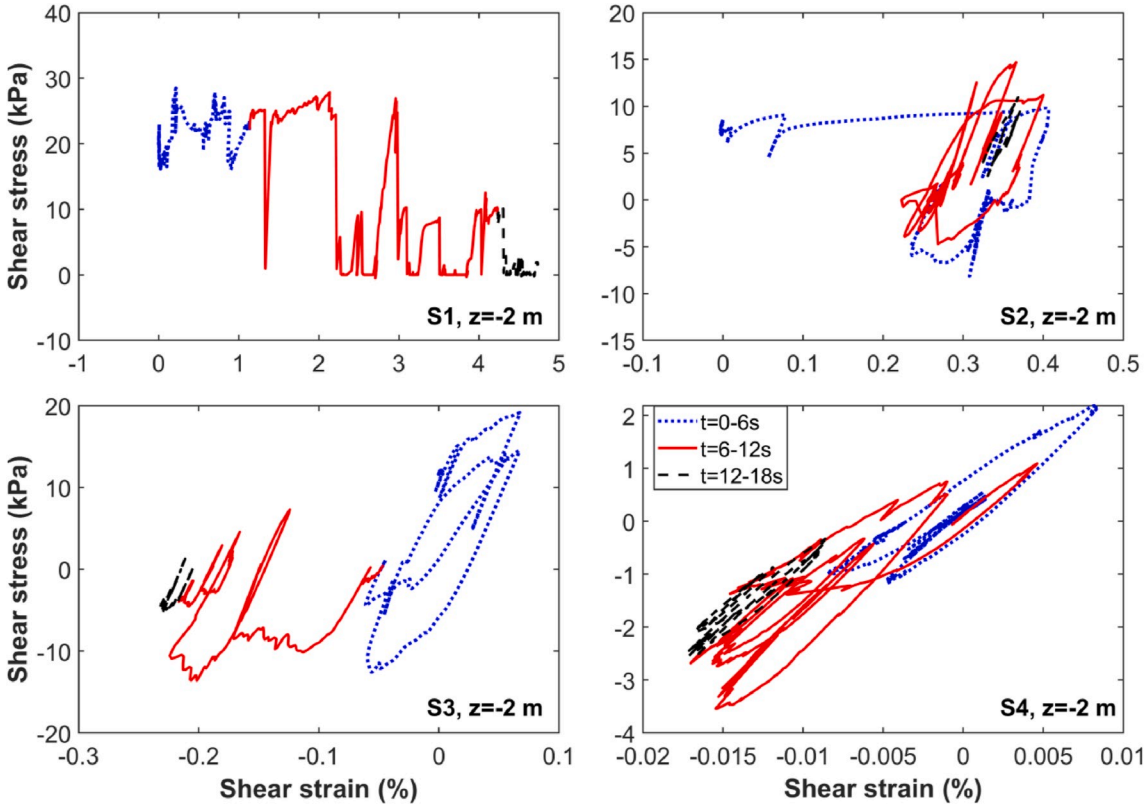


**Fig. 14.** Shear stress-strain responses at monitoring points and depth z = −2 m in Caisson Case 1 for different time periods.

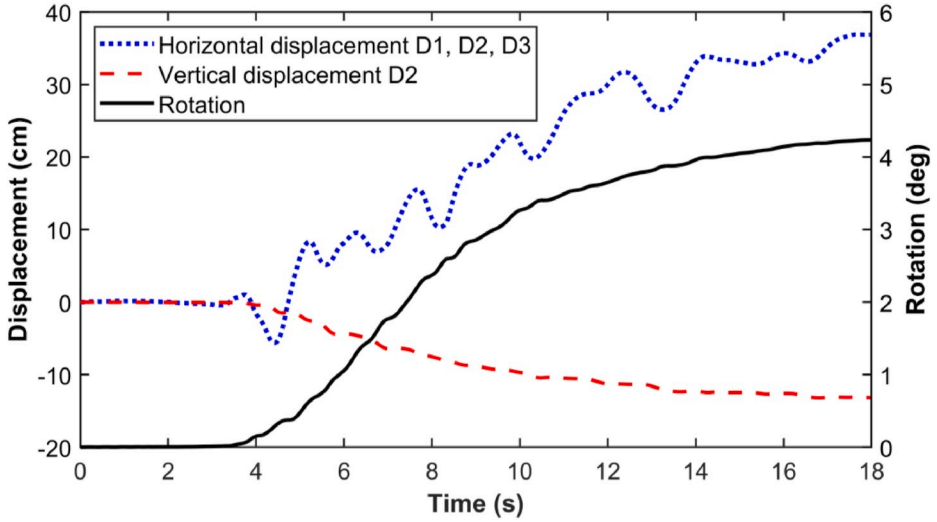


**Fig. 15.** Caisson Case 1 – Time histories of horizontal, vertical and rotational displacements of caisson.

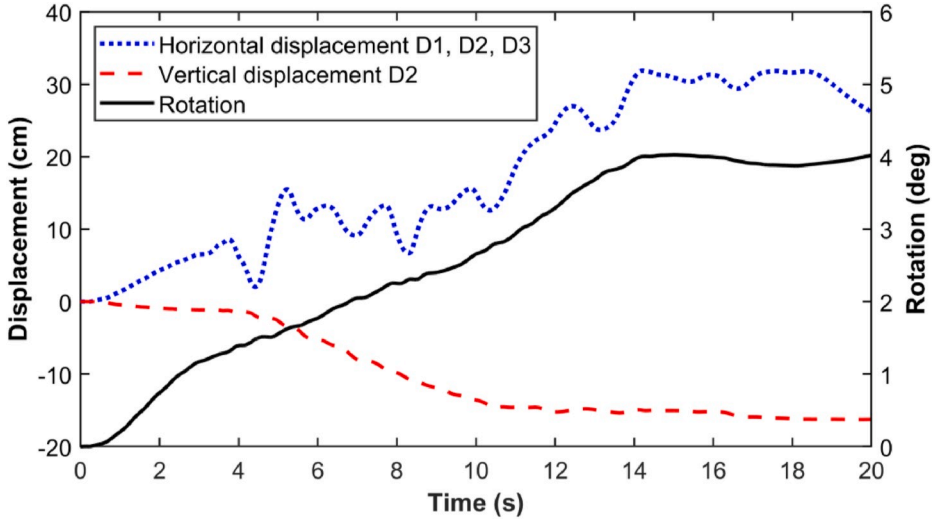


**Fig. 16.** Caisson Case 2 – Time histories of horizontal, vertical and rotational displacements of caisson.

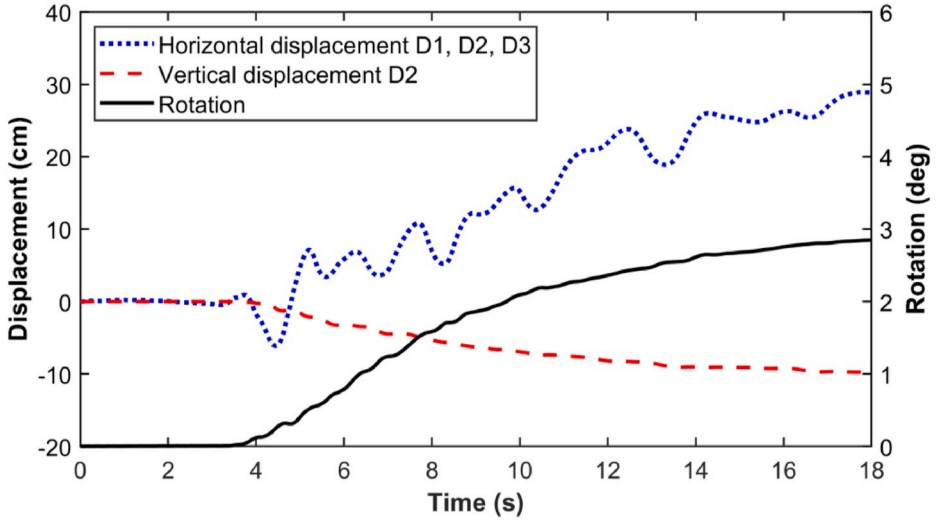


**Fig. 17.** Caisson Case 3 – Time histories of horizontal, vertical and rotational displacements of caisson.

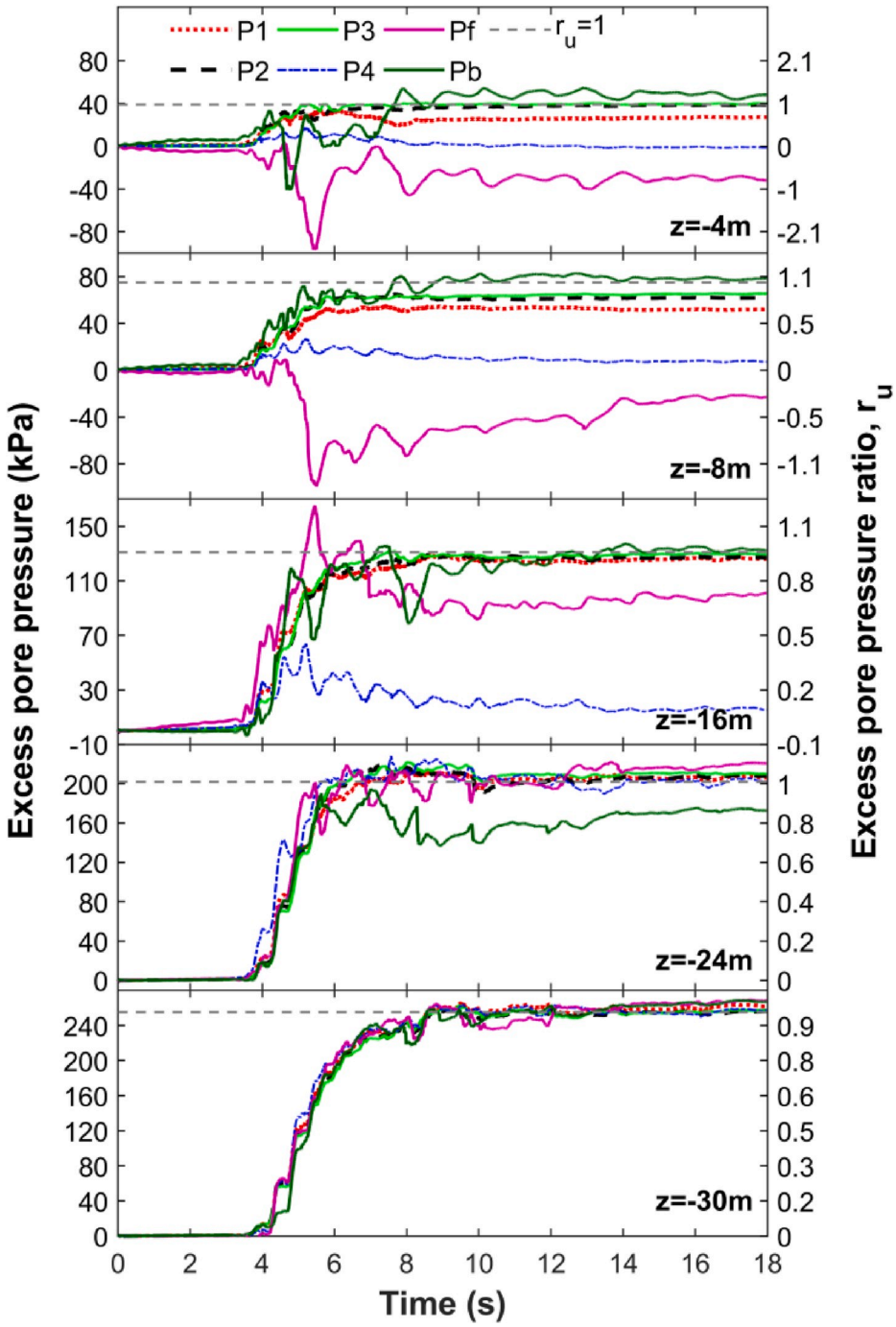


**Fig. 18.** Time histories of excess pore pressure at monitoring points in Monopile Case1 (Pb and Pf are monitoring points at 1.3 m behind and in front of the pile).

intensification of shaking and pore pressure generation (red segments) and finally to small cyclic loops reflecting the full liquefaction state and reduction of shaking (black segments).

Fig. 15 shows the time histories of the horizontal, vertical and rotational displacements of the caisson in Case 1. It can be observed that the permanent rotation of the caisson (about 4 deg.) exceeds by far the acceptable tilt (0.25–0.5 deg.). Also, one can observe the permanent horizontal displacement of about 30 cm and downward sinking of 10 cm during the shaking.

Figs. 16 and 17 illustrate the same set of results for caissons Case 2 and Case 3. As shown in Fig. 16, both displacements and tilt initiate faster when the cyclic wind load is applied to the model in Case 2. Nonetheless, almost the same permanent rotation and horizontal displacements are reached in Cases 1 and 2 whereas, the caisson experiences slightly higher sinking in Case 2. As expected, increasing the diameter of the caisson to 15 m in Case 3 leads to lower rotations (Fig. 17) compared to the other cases.

### 4.2. OWT on monopiles

Fig. 18 illustrates the computed time histories of excess pore water pressure at different points and depths in the soil medium for Case 1. The plots in the figure confirm that the excess pore pressure is always lower inside the pile (point P4) which as discussed earlier is believed to be due to the kinematic confinement by the monopile. The figure also includes the pore water pressures at the points Pb and Pf at the back and front of

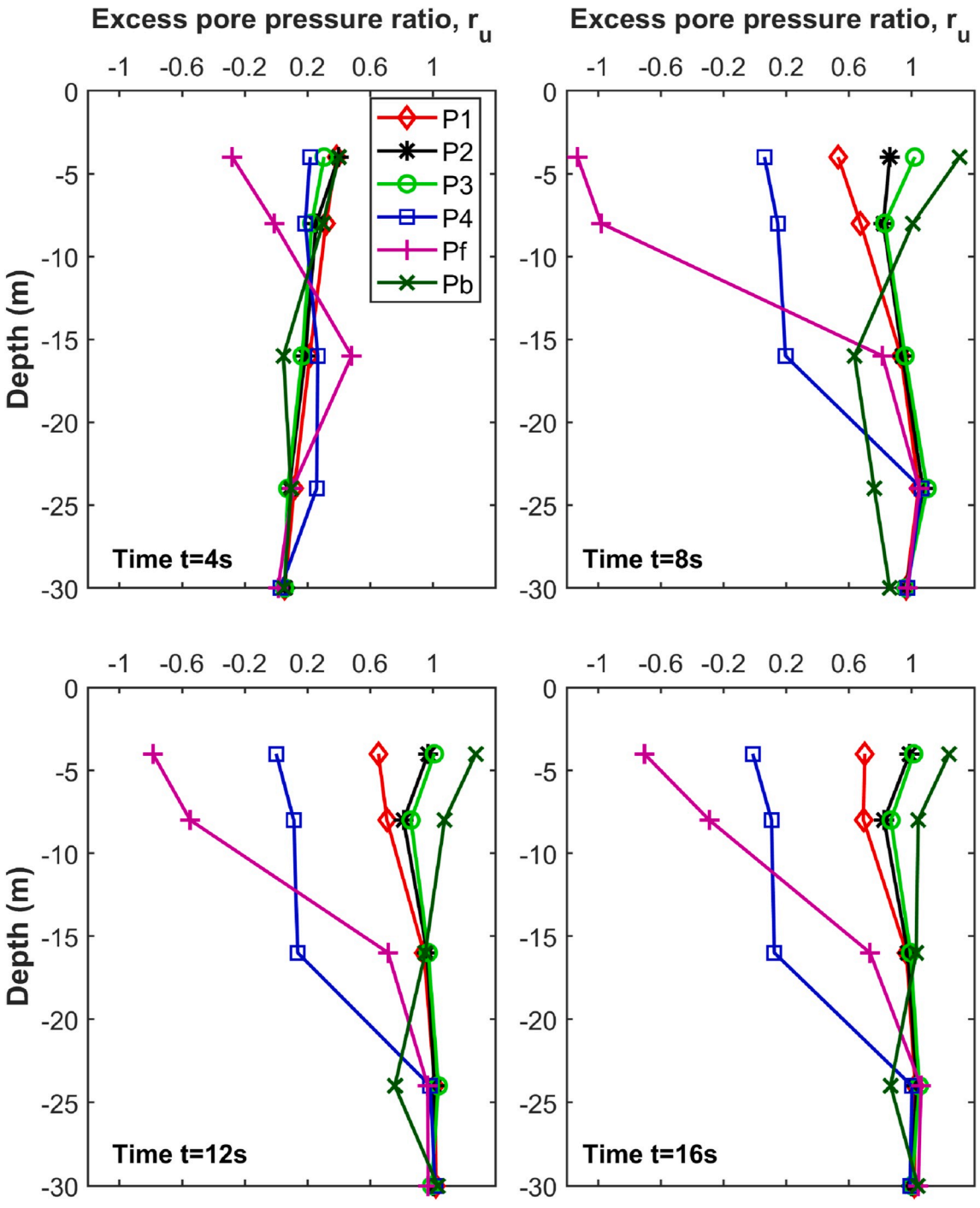


**Fig. 19.** Profiles of $r_u$ at different monitoring points and time instances in Monopile (Pb and Pf are monitoring points at 1.3 m behind and in front of the pile).

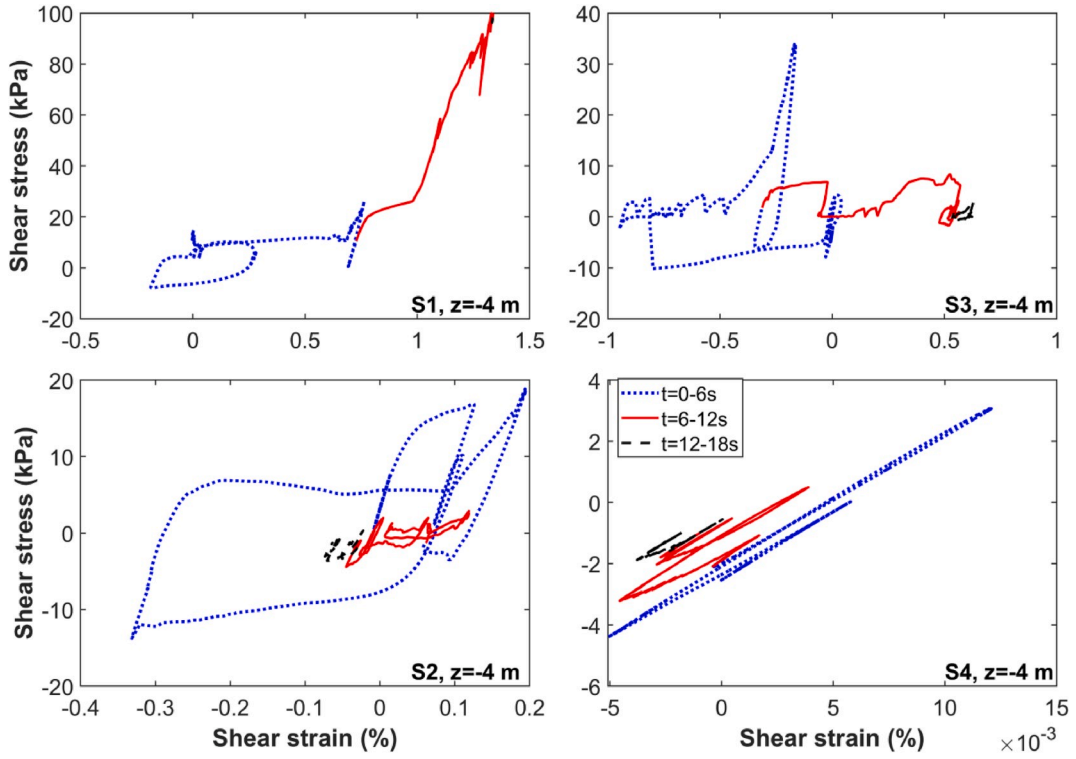


**Fig. 20.** Shear stress-strain responses at monitoring points and depth z = −4 m in Monopile Case1 for different time periods.

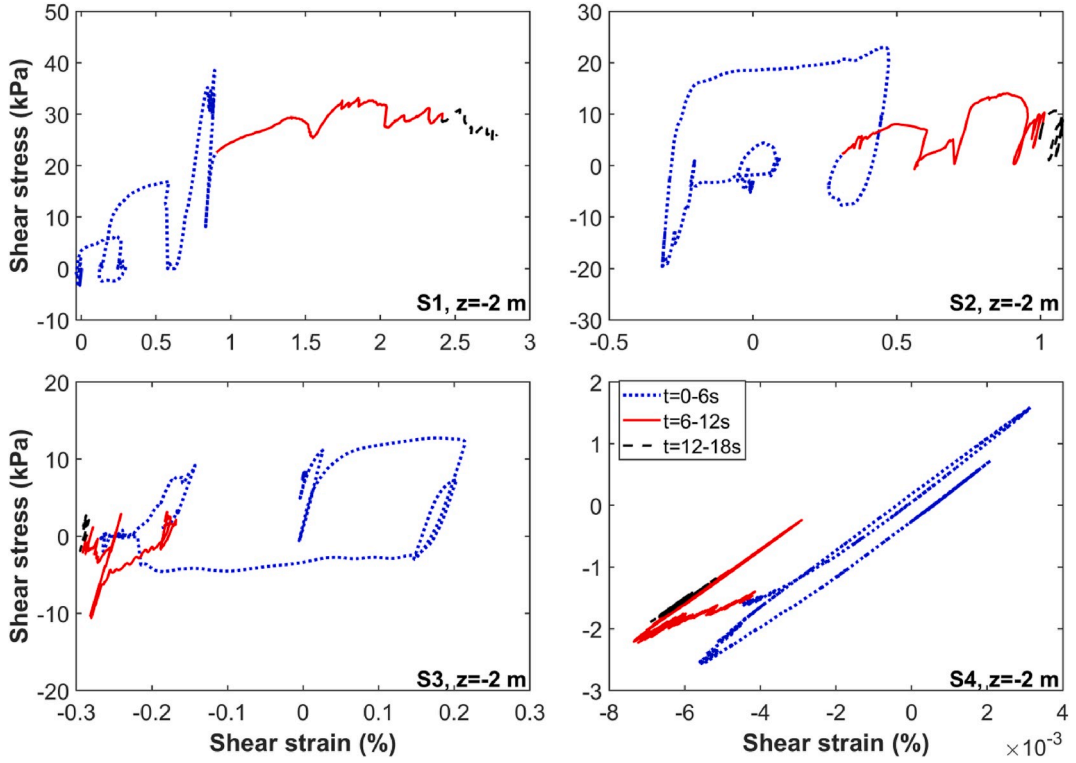


**Fig. 21.** Shear stress-strain responses at monitoring points and depth z = −2 m in Monopile Case1 for different time periods.

the monopile. Fig. 19 displays the profile of $r_u$ with depth at the monitoring points at four instances 4, 8, 12 and 16 s for Case 1. This figure gives a useful insight into the progression of pore pressure generation during ground shaking.

Figs. 20 and 21 display the shear stress-strain responses at monitoring points at depths z = −4 m and z = −2 m during the earthquake shaking. As in the case of caissons (Figs. 13 and 14), different colors are used to differentiate between the responses in the time windows 0–6 s, 6–12 s and 12–18 s. The plots show clearly again the shift in the response during shaking from more conventional hysteretic and

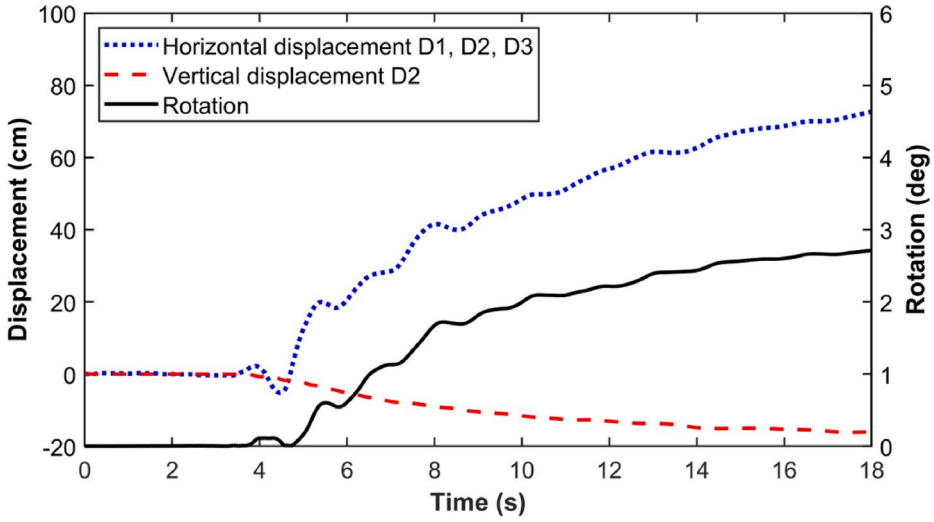


**Fig. 22.** Monopile Case 1 – Time histories of horizontal, vertical and rotational displacements of monopile.

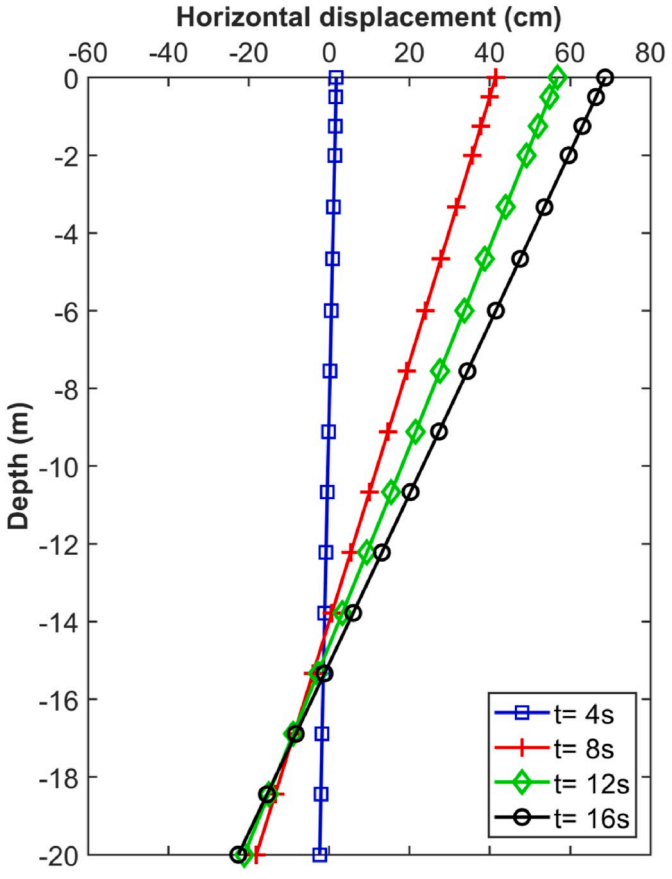


**Fig. 23.** Monopile Case 1 - Profile of horizontal displacement of monopile with depth at four time steps.

symmetrical responses to large yielding due to intensification of pore pressure generation and finally to small cyclic loops reflecting full liquefaction state and lower shaking.

Fig. 22 presents the horizontal, vertical and rotational displacements of the monopile in Case 1. The permanent rotation of the pile (about 3 deg.) exceeds the allowable tilt (0.25–0.5 deg.) which means that although the structure does not collapse by the shaking and liquefaction, it is considered unfit for use after the earthquake. While similar permanent lateral and rotational movements have resulted in this case and caisson model with D = 15 m (Case 3), larger sinking can be observed in Monopile Case 1. The reason is believed to be due to the higher weight of the monopile . To provide an insight into the evolution of pile deformation during the earthquake, the profile of the horizontal displacements of the pile with depth is presented in Fig. 23 at time instances 4, 8, 12 and 16 s. The figure clearly shows the gradual tilt of the pile and its rotation around a point close to the pile tip as the shaking continues.

Figs. 24 and 25 present the results of analysis for Monopile Case 2. They indicate slightly lower permanent rotation of the pile in this case (2.4 deg. vs. 2.8 deg. in Case 1), which is believed to be due to the higher length of the pile; however, the permanent horizontal displacement has increased from 70 cm to 80 cm.

Fig. 26 displays the results of analyses for monopile Case 3. The figure indicates lower rotational and lateral displacements in this case where cyclic wind load is applied to the top of the tower. From these results one can conclude that representation of wind load by a constant load during earthquake shaking might present a more critical condition than inclusion of the cyclic component of the wind load. On the other hand, it is interesting to note that the cyclic component has slightly increased the sinking (from 10 to 13 cm).

Fig. 27 shows the same set of results for the monopile in Case 4 where the pile length is increased such that it penetrates 9 m into the dense Ottawa sand layer. This case indicates the lowest transient and permanent rotations (1.6 deg.) while the calculated permanent horizontal displacement is close to that in Case 2. Moreover, a lower sinking can be observed in this case in comparison with the other cases. This is because the pile tip rests on a dense sand layer which provides more resistance to vertical downward displacement of the structure.

The results for Case 5 (which includes a layer of surficial non-liquefiable sand representing s scour protection around the monopile) indicate that this measure reduces both the horizontal and rotation of the pile (for brevity, the figures of the results are not included). The permanent rotation decreases to the same level as in Case 2 (2.5 deg.) where the pile's length is 25 m and horizontal displacements at the mudline decrease to 1, 36, 50 and 60 cm at times 4, 8, 12 and 16 s, respectively. These are encouraging results that point to the use of scour protection in sandy sites as a potential measure against excessive tilt of monopiles in liquefiable soils. Dedicated numerical studies, preferably backed by model testing in centrifuge, are needed to assess more accurately the potential benefits of soil replacement in liquefiable soil.

As discussed earlier, in all the above cases excessive rotation of the foundation occurs due to liquefaction. This is primarily caused by the

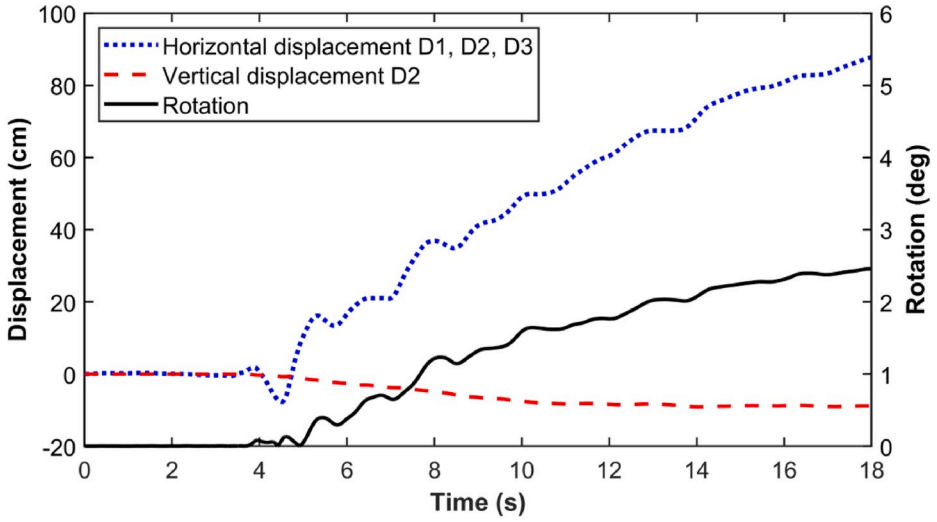


**Fig. 24.** Monopile Case 2 – Time histories of horizontal, vertical and rotational displacements of monopile.

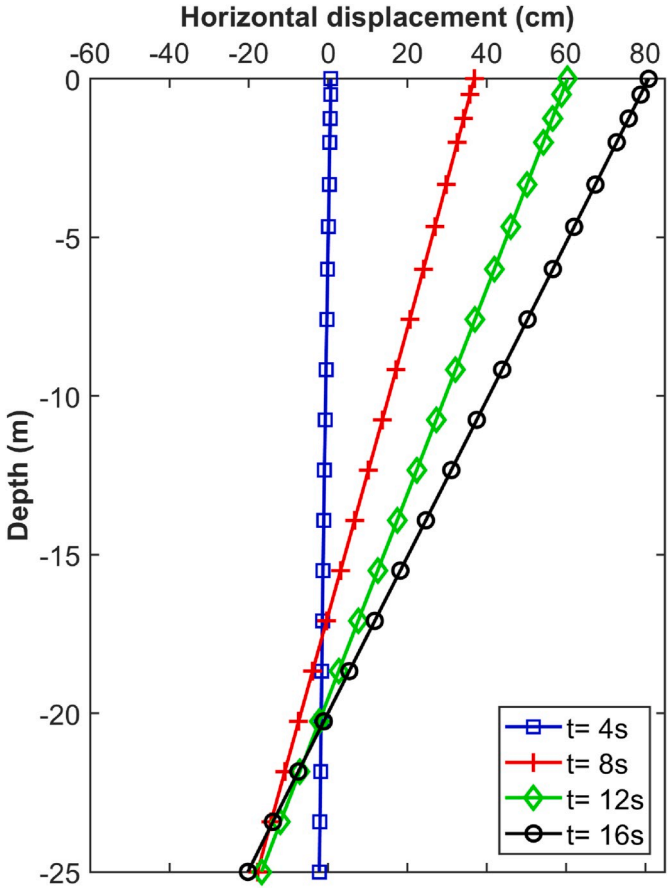


**Fig. 25.** Monopile Case 2 - Profile of horizontal displacement of monopile with depth at four time steps.

static lateral wind load, which makes the loading unsymmetrical. To confirm this, Case 6 was considered in which the response of the monopile in Case 2 subjected to solely earthquake shaking (loading type C) was computed. The results of analyses for monopile Case 6 are shown in Fig. 28 that indicate that the permanent lateral and rotational displacements of the OWT subjected to only earthquake loading are very small (a similar analysis was carried out for the caisson Case 3; the results for the caisson are comparable and are thus not shown for brevity). It is unlikely that a strong earthquake occurs during a heavy storm; therefore, in view of these results, it is important to use a realistic wind/wave loading representative of normal operating conditions in a seismic design.

Figs. 29 and 30 display the excess pore pressures and displacements of the pile in Case 2 for an earthquake shaking reduced to 30% of the cases considered above. The results in Fig. 29 show that Although the soil still liquefies at most of the points even under the reduced shaking, the pore pressure is generated more slowly in this case and it takes longer for the soil to reach the full liquefaction state. As shown in Fig. 30, the permanent tilt of the pile is remarkably lower (by about 80%) than when the maximum earthquake shaking is applied. Although the rotation has not exceeded the maximum allowable value (i.e 0.5 deg), it is very close to the limit, revealing that asymmetrical loading due to the wind load results in considerable rotational displacements of OWT foundations in liquefiable soil even under moderate ground shakings.

## 5. Summary and conclusions

The effect of liquefaction on the performance of shallow (caisson) and deep (monopile) foundations for OWTs under combined actions of ground shaking and static/cyclic wind loads has been studied in this paper. To compare the results of the considered cases, the excess pore water pressure and shear stress-strain responses in the soil medium, as well as horizontal and rotational movements of the caisson/monopile, have been computed and presented.

The analyses indicate that the pore pressure generation inside the pile/caisson is lower than outside. This is believed to be due to the kinematic confinement provided by the foundation.

The numerical results indicate that extensive permanent rotations of caissons could occur due to liquefaction; however, the rotational movements diminish as the diameter of the caisson increases. Similarly, it has been observed that the rotation of monopiles during the earthquake shaking diminishes as the length of the pile increases. In particular, when the monopile has an embedded length in a nonliquefiable soil, like a dense sand layer, both rotation and downward sinking of the pile decrease considerably. Generally, vertical displacements of monopiles have been higher than those of caissons during the ground shaking due to their larger weight. Both permanent rotational and horizontal displacements of monopiles decrease because of replacing the liquefiable sand around the pile with non-liquefiable sand. The replacement can be in conjunction with the use of non-liquefiable sand for scour protection. The asymmetrical loading due to the action of wind

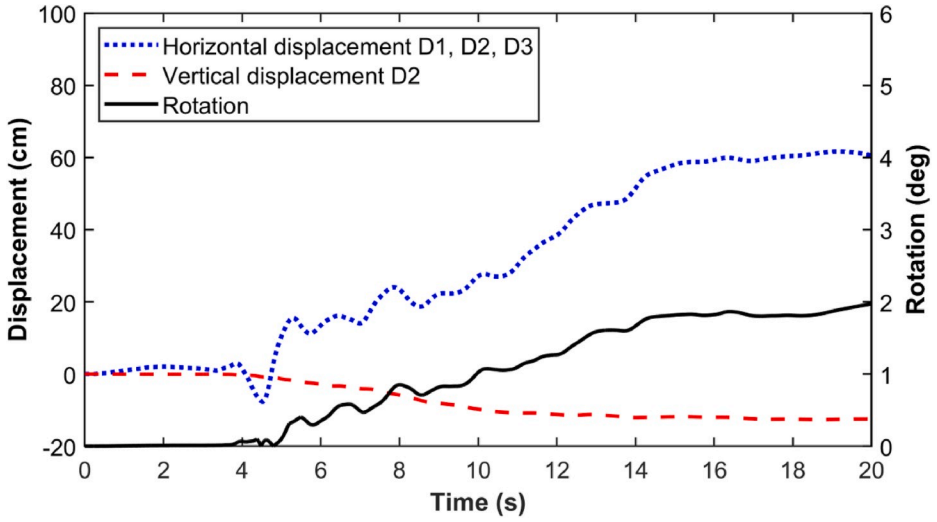


**Fig. 26.** Monopile Case 3 – Time histories of horizontal, vertical and rotational displacements of monopile.

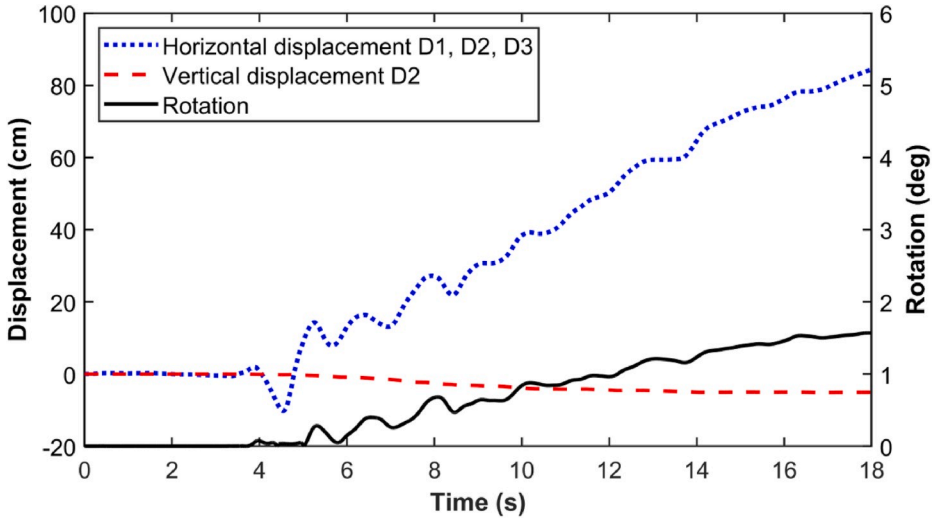


**Fig. 27.** Monopile Case 4 – Time histories of horizontal, vertical and rotational displacements of monopile.

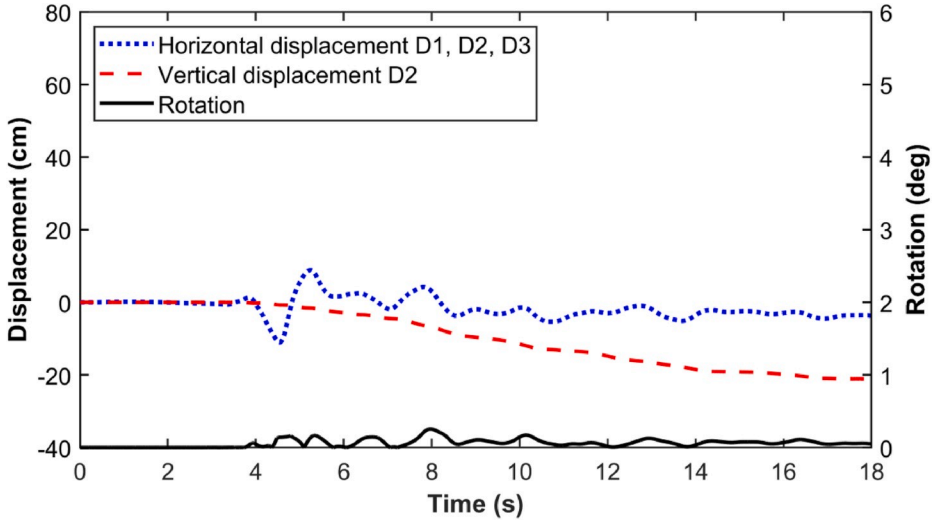


**Fig. 28.** Time histories of horizontal, vertical and rotational displacements of monopile in Case 6 subjected to loading type C (only earthquake shaking).

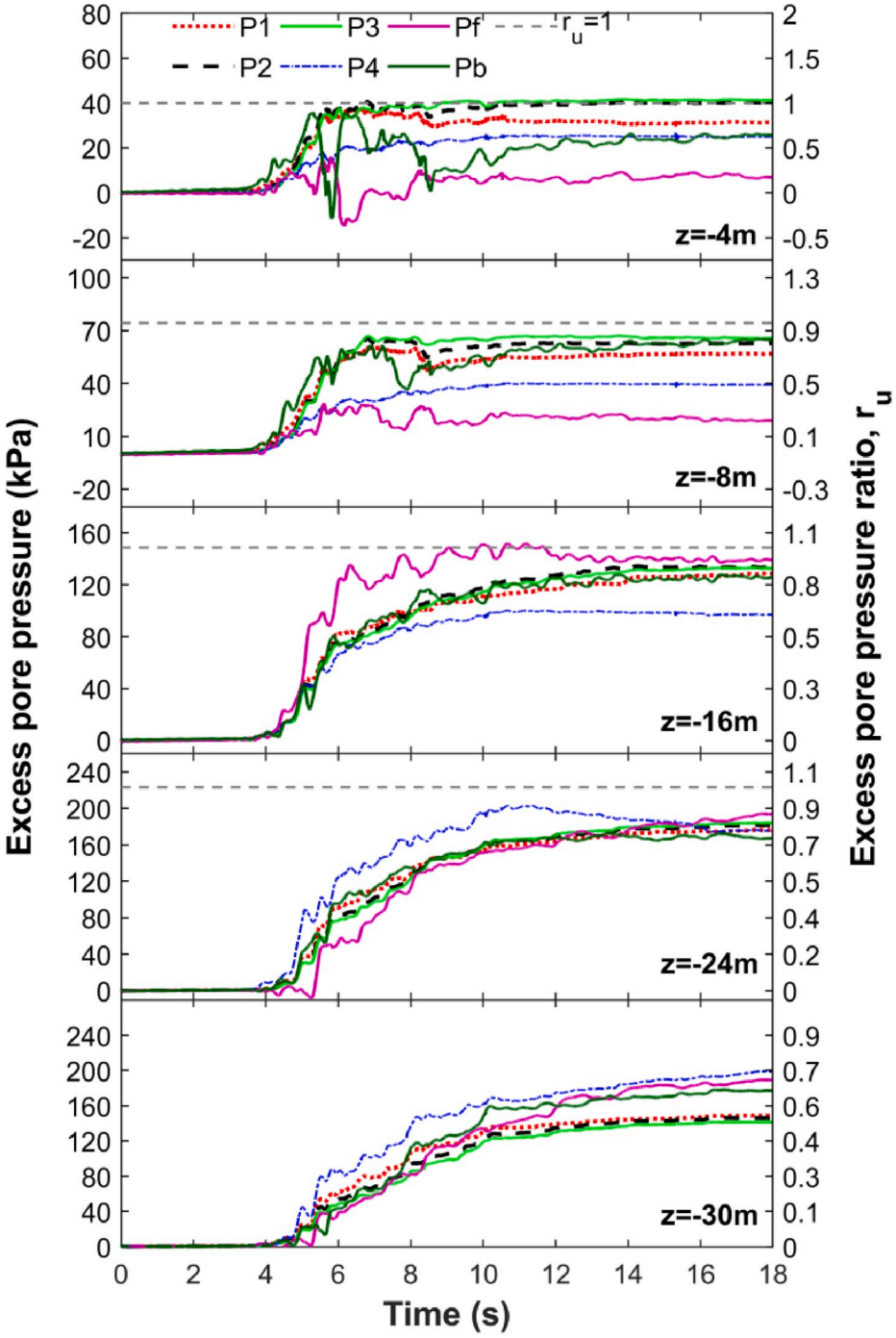


**Fig. 29.** Time histories of excess pore pressure at monitoring points in Monopile Case 2 subjected to shaking reduced to 30% (Pb and Pf are monitoring points at 1.3 m behind and in front of the pile).

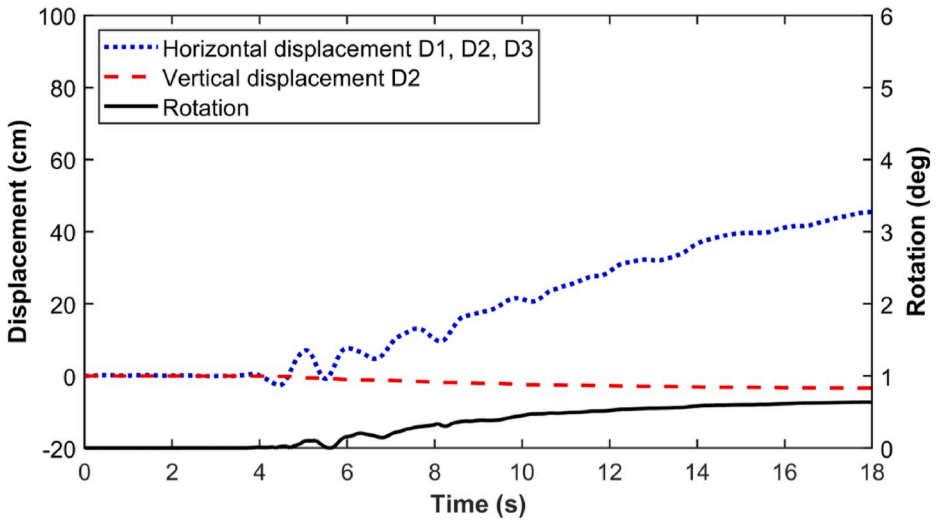


**Fig. 30.** Time histories of horizontal, vertical and rotational displacements of monopile in Case 2 subjected to shaking reduced to 30%.

load during earthquake shaking can lead to large rotation of OWT foundations in liquefiable soil even under moderate ground shakings threatening the functionality and stability of these structure.

## Acknowledgment

The authors would like to thank the three anonymous reviewers for their valuable and constructive comments that have improved the quality of this paper.

## Appendix A. Supplementary data

Supplementary data to this article can be found online at https://doi.org/10.1016/j.soildyn.2020.106213.

## References

[1] International Renewable Energy Agency Offshore innovation widens renewable energy options. 2018. ISBN: 978-92-9260-079-2.
[2] Kaynia AM. Seismic considerations in design of offshore wind turbines. Soil Dynam Earthq Eng 2018. https://doi.org/10.1016/j.soildyn.2018.04.038.
[3] Asareh MA, Schonberg W, Volz J. Effects of seismic and aerodynamic load interaction on structural dynamic response of multi-megawatt utility scale horizontal axis wind turbines. Renew Energy 2016;86:49–58. https://doi.org/10.1016/j.renene.2015.07.098.
[4] Smith V, Mahmoud H. Multihazard assessment of wind turbine towers under simultaneous application of wind, operation, and seismic loads. J Perform Constr Facil ASCE 2016;4016043(6):30. https://doi.org/10.1061/(ASCE)CF. 1943-5509.0000898.
[5] Kjørlaug RA, Kaynia AM, Elgamal A. Seismic response of wind turbines due to earthquake and wind loading. In: Proceedings of 9th international conference on structural dynamics, EURODYN 2014. Porto, Portugal; 2014.
[6] De Alba P, Seed HB, Chan CK. Sand liquefaction in large scale simple shear tests. J. Geotechnical Eng Div ASCE 1976;102:909–27.
[7] Idriss IM, Boulanger RW. Soil liquefaction during earthquakes. Monograph MNO-12. Oakland, 10/02. Department of civil and environmental engineering, university of California davis. California, USA: Center for Geotechnical Modeling; 2010.
[8] Idriss IM, Boulanger RW. SPT-based liquefaction triggering procedures. Report UCD/CGM-10/02. Department of civil and environmental engineering, university of California davis. California, USA: Center for Geotechnical Modeling; 2010.
[9] Boulanger RW, Idriss IM (2). CPT-based liquefaction triggering procedure. J Geotech and Geoenviron Eng ASCE, 142; 2015. https://doi.org/10.1061/(ASCE)GT. 1943-5606.0001388.
[10] Rapti I, Lopez-Caballero F, Modaressi-Farahmand-Razavi A, Foucault A, Voldoire F. Liquefaction analysis and damage evaluation of embankment-type structures. Acta Geotech 2018;13(5):1041–59. https://doi.org/10.1007/s11440-018-0631-z.
[11] Ziotopoulou K, Montgomery J. Numerical modeling of earthquake-induced liquefaction effects on shallow foundations. In: 16th world conference on earthquake engineering. Santiago: Chile; 2017. 16WCEE 2017.
[12] Sinha SK, Ziotopoulou K, Kutter BL. Parametric study of liquefaction induced downdrag on axially loaded piles. In: 7th international conference on earthquake geotechnical engineering. Roma: Italy; 2019.
[13] Kallehave D, Thilsted CL, Liingaard M. Modification of the API p-y formulation of initial stiffness of sand. In: Proceedings of offshore site investigation and geotechnics: integrated technologies – present and future. London: UK. Society of Underwater Technology; 2012. p. 465–72.
[14] Bhattacharya S, Cox JA, Lombardi D, Wood DM. Dynamics of offshore wind turbines supported on two foundations. Proc Inst Civ Eng Geotech Eng 2013;166:159–69.
[15] Lombardi D, Bhattacharya S, Wood DM. Dynamic soil–structure interaction of monopile supported wind turbines in cohesive soil. Soil Dynam Earthq Eng 2013;49:165–80.
[16] Damgaard M, Bayat M, Andersen LV, Ibsen LB. Assessment of the dynamic behaviour of saturated soil subjected to cyclic loading from offshore monopile wind turbine foundations. Comput Geotech 2014;61:116–26.
[17] Thieken K, Achmus M, Lemke K. Evaluation of a new p-y approach for piles in sand with arbitrary dimensions. In: Proceedings of 3rd international symposium on frontiers in offshore geotechnics, Oslo, Norway. p. 705–710.
[18] Thieken K, Achmus M, Lemke K. A new static p-y approach for piles with arbitrary dimensions in sand. Geotechnik 2015;38(4):267–88.
[19] Byrne BW, McAdam RA, Burd HJ, Houlsby GT, Martin CM, Gavin K, et al. Field testing of large diameter piles under lateral loading for offshore wind applications. In: Proceedings of the 16th European conference on soil mechanics and geotechnical engineering, Edinburgh, UK. p. 1255–1260.
[20] Zdravkovic L, Taborda DMG, Potts DM, Jardine RJ, Sideri M, Schroeder FC, et al. Numerical modelling of large diameter piles under lateral loading for offshore wind applications. In: Proceedings of 3rd international symposium on frontiers in offshore geotechnics, Oslo, Norway.
[21] Byrne BW, McAdam RA, Burd HJ, Houlsby GT, Martin CM, Zdravkovic L, et al. New design methods for large diameter piles under lateral loading for offshore wind applications. In: Proceedings of 3rd international symposium on frontiers in offshore geotechnics, Oslo, Norway. p. 705–710.
[22] Versteijlen WG, Metrikine AV, van Dalen KN. A method for identification of an effective winkler foundation for large-diameter offshore wind turbine support structures based on in-situ measured small-strain soil response and 3D modelling. Eng Struct 2016.
[23] Byrne BW, McAdam RA, Burd HJ, Houlsby GT, Martin CM, Beuckelaers WJAP, Zdravkovic L, Taborda DMG, Potts DM, Jardine RJ, Ushev E, Liu T, Abadias D, Gavin K, Igoe D, Doherty P, Skov Gretlund J, Pacheco Andrade M, Muir Wood A, Schroeder FC, Turner S, Plummer MAL. PISA: new design methods for offshore wind turbine monopiles. In: Proceedings of the 8th international conference on offshore site investigation and geotechnics, vol. 1. London: Royal Geographical Society; 2017. p. 142–91.
[24] Achmus M, Kuo Y-S, Abdel-Rahman K. Behavior of monopile foundations under cyclic lateral load. Comput Geotech 2009;36(5):725–35.
[25] LeBlanc C, Houlsby GT, Byrne BW. Response of stiff piles in sand to long-term cyclic lateral loading. Geotechnique 2010;60(2):79–90.
[26] Bienen B, Dührkop J, Grabe J, Randolph MF, White DJ. Response of piles with wings to monotonic and cyclic lateral loading in sand. J Geotech Geoenviron Eng 2011;138(3):364–75.
[27] Rudolph C, Bienen B, Grabe J. Effect of variation of the loading direction on the displacement accumulation of large-diameter piles under cyclic lateral loading in sand. Can Geotech J 2014;51(10):1196–206.
[28] Markou AA, Kaynia AM. Nonlinear soil-pile interaction for offshore wind turbines. Wind Energy 2018. https://doi.org/10.1002/we.2178.
[29] Boulanger RW, Curras CJ, Kutter BL, Wilson DW, Abghari A. Seismic soil-pile structure interaction experiments and analysis. 750–9 J Geotech Geoenviron Eng ASCE 1999 1999;125(9):125. https://doi.org/10.1061/(asce)1090-0241. 9(750).

[30] Cuéllar P, Mira P, Pastor M, Fernández-Merodo JA, Baeßler M, Rücker W. A numerical model for the transient analysis of offshore foundations under cyclic loading. Comput Geotech 2014;59:75–86.
[31] Corciulo S, Zanoli O, Pisano F. Transient response of offshore wind turbines on monopiles in sand: role of cyclic hydro–mechanical soil behavior. Comput Geotech 2017;83:221–38.
[32] Yang CB, Wang R, Zhang JM. Seismic analysis of monopile supported offshore wind turbine. Chongqing, China: International Conference on Geotechnical and Earthquake Engineering; 2018.
[33] Kementzetzidis E, Corciulo S, W G Versteijlen, Pisanò F. Geotechnical aspects of offshore wind turbine dynamics from 3D non-linear soil-structure simulations. Soil Dynam Earthq Eng 2019;120:181–99. https://doi.org/10.1016/j.soildyn.2019.01.037.
[34] Zhu B, Byrne BW, Houlsby GT. Long term lateral cyclic response of suction caisson foundations in sand. Journal of Geotechnical and Geoenvironmental Engineering, ASCE 2013;139(1):73–83.
[35] Kazemi Esfeh P, Kaynia AM. Numerical modeling of liquefaction and its impact on anchor piles for floating offshore structures. Soil Dynam Earthq Eng 2019:127.
[36] Kourkoulis RS, Lekkakis PC, Gelagoti FM, Kaynia AM. Suction caisson foundationsfor offshore wind turbines subjected to wave and earthquake loading: effect of soil foundation interface. Geotechnique 2014;64(3):171–85. https://doi.org/10.1680/geot.12.P.179.
[37] Yang Z, Lu J, Elgamal A. OpenSees soil models and solid-fluid fully coupled elements: user's manual. Department of Structural Engineering. California, USA: University of California San Diego; 2008.
[38] Dafalias YF, Manzari MT. Simple plasticity sand model accounting for fabric change effects. 2004 J Eng Mech 2004;130(6):622–34. https://doi.org/10.1061/(ASCE)0733-9399. 130:6(622).
[39] Taiebat M, Jeremić B, Dafalias YF, Kaynia AM, Cheng Z. Propagation of seismic waves through liquefied Soils. Soil Dynam Earthq Eng 2010;30(4):236–57. April 2010.
[40] Boulanger RW, Ziotopoulou K. PM4Sand (Version 3): a sand plasticity model for earthquake engineering applications. Report UCD/CGM-15/01. University of California Davis. California, USA: Center for Geotechnical Modeling; 2015.
[41] Andrianopoulos KI, Papadimitriou AG, Bouckovalas GD. Bounding surface plasticity model for the seismic liquefaction analysis of geostructures. Soil Dynam Earthq Eng 2010;30(10):895–911.
[42] Manzari MT, Arulanandan K. Numerical predictions for model no. 1. In: Arulanandan K, Scott RF, editors. Verification of numerical procedures for the analysis of soil liquefaction problems. Rotterdam, Netherlands: A.A. Balkema; 1993. p.179–185.
[43] Ghofrani A, Arduino P. Prediction of LEAP centrifuge tests results using a pressure-dependent bounding surface constitutive model. Soil Dynam Earthq Eng 2018;113:758–70. https://doi.org/10.1016/j.soildyn.2016.12.001.
[44] Ziotopoulou K. Seismic response of liquefiable sloping ground: class A and C numerical predictions of centrifuge model responses. Soil Dynam Earthq Eng 2018;113:744–57. https://doi.org/10.1016/j.soildyn.2017.01.038.
[45] Ekstrom LT, Ziotopoulou K. Seismic response of liquefiable sloping ground: validation of class B predictions against the LEAP centrifuge tests. In: Geotechnical frontier 2017. Orlando: Florida; 2017. https://doi.org/10.1061/9780784480489.034.
[46] Ramirez J, Barrero A R, Chen L, Dashti S, Ghofrani A, Taiebat M, Arduino P. Site response in a layered liquefiable deposit: evaluation of different numerical tools and methodologies with centrifuge experimental results. J Geotech Geoenviron ASCE 2018;144(10). https://doi.org/10.1061/(ASCE)GT. 1943-5606.0001947.
[47] Kutter BL, Carey TJ, Hashimoto T, Manzari MT, Vasko A, Zeghal M, Armstrong RJ. LEAP database for verification, validation, and calibration of codes for simulation of liquefaction. In: 6th international conference on earthquake geotechnical engineering. Christchurch: New Zealand; 2015.
[48] Elgamal A, Yang Z, Parra E. Computational modeling of cyclic mobility and post-liquefaction site response. Soil Dynam Earthq Eng 2002;22(4):259–71. https://doi.org/10.1016/S0267-7261(02)00022-2.
[49] Ramirez J, et al. Seismic performance of a layered liquefiable site: validation of numerical simulations using centrifuge modeling. In: Geotechnical frontiers 2017. Reston, VA: ASCE: Geotechnical Special Publication; 2017. p. 281.
[50] Kirkwood P, Dashti S. A centrifuge study of seismic structure-soil-structure interaction on liquefiable ground and implications for design in dense urban areas. Earthq Spectra 2018;34(3):1113–34. https://doi.org/10.1193/052417EQS095M.
[51] Biot MA. General theory of three-dimensional consolidation. J Appl Phys 1941;12(2):155–64. https://doi.org/10.1063/1.1712886.
[52] Zienkiewicz OC, Shiomi T. Dynamic behavior of saturated porous media, the generalized Biot formulation and its numerical solution. Int. J. Numer. Methods Geomech 1984;8(1):71–96. https://doi.org/10.1002/nag.1610080106.
[53] Detournay E, Cheng AD. Fundamentals of poroelasticity. In: Fairhurst C, editor. Comprehensive rock engineering: principles, practice & projects, analysis and design methods. vol. 2. , Oxford: Pergamon Press; 1993. p. 113–71.
[54] Manzari MT, Dafalias YF. A critical state two-surface plasticity model for sands. Geotechnique 1997;47(2):255–72. https://doi.org/10.1680/geot.1997.47.2.255.
[55] Jonkman J, Butterfield S, Musial W, Scott G. Definition of a 5-mw reference wind turbine for offshore system development. National Renewable Energy Laboratory 2009.
[56] Løken IB, Kaynia AM. Effect of foundation type and modelling on dynamic response and fatigue of offshore wind turbines. Wind Energy 2019.
[57] Krathe VL, Kaynia AM. Implementation of a non-linear foundation model for soil-structure interaction analysis of offshore wind turbines in FAST. Wind Energy 2017;20:695–712.